Mathematical Biosciences 365 (2023) 109086

Contents lists available at ScienceDirect

Mathematical Biosciences

journal homepage: www.elsevier.com/locate/mbs

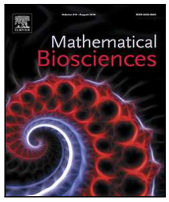

Original Research Article

Effect of cross-immunity in a two-strain cholera model with aquatic component

Leah LeJeune[1], Cameron Browne *

Department of Mathematics, University of Louisiana at Lafayette, Lafayette, LA, USA

ARTICLE INFO

Keywords:
Cholera
Cross-immunity
Serotype cycling
Environmental transmission
Disease persistence

ABSTRACT

The bacteria *Vibrio cholerae* relies heavily upon an aquatic reservoir as a transmission route with two distinct serotypes observed in many recent outbreaks. In this paper, we extend previously studied ordinary differential equation epidemiological models to create a two-strain $SIRP$ (susceptible-infectious-recovered-pathogen) system which incorporates both partial cross-immunity between disease strains and environmental pathogen transmission. Of particular interest are undamped anti-phase periodic solutions, as these display a type of coexistence where strains routinely switch dominance, and understanding what drives this switch can optimize the efficiency of the host population's control measures against the disease. We derive the basic reproduction number R_0 and use stability analysis to examine the disease free and single-strain equilibria. We formulate a unique coexistence equilibrium and prove uniform persistence of both strains when $R_0 > 1$. In addition, we simulate solutions to this system, along with seasonally forced versions of the model with and without host coinfection. Cross-immunity and transmission pathways influence damped or sustained oscillatory dynamics, where the presence of seasonality can modify, amplify or synchronize the period and phase of serotypes, driving epidemic waves. Cycling of serotypes over large time intervals, similar to observed data, is found for a range of cross-immunity levels, and the inclusion of coinfection in the model contributes to sustained anti-phase periodic solutions.

1. Introduction

Cholera, unlike many diseases, can survive, proliferate, and compete in the aquatic environment, a necessary factor to consider when modeling its long-term dynamics [1]. Previous susceptible-infected-recovered-pathogen ($SIRP$) ordinary differential equations models have examined a single cholera strain invading a host population while considering the pathogen environmental concentration [2–6]. Multi-strain disease models of cholera and other infectious diseases, with multiple serotypes conferring some degree of cross-immunity against secondary infection from a strain other than the strain from the primary infection, have also been extensively examined, but without considering an environmental component [7–9]. These models may consider strain differences in environmental and host fitness parameters, as well as partial cross-immunity. It is necessary, however, to consider strain diversity and analyze multi-strain models which incorporate both cross-immunity factors and pathogen environmental compartments to better understand transmission dynamics and long-term behavior (e.g. coexistence versus competitive exclusion) of circulating serotypes for cholera [2,10]. In this paper, we extend the single-strain model to a two-strain $SIRP$ cholera model, considering two distinct serotypes of the bacteria, Ogawa and Inaba, and analyze equilibrium, stability and uniform persistence of solutions to the system.

The Ogawa and Inaba serotype strains of cholera have been observed to display cyclic behavior within a given host population [7]. This has been analyzed in models excluding the environmental component [7–9], and here we study cyclic behavior in our extended model which includes the environmental component. The cyclic behavior that is of particular interest in the presence of both serotypes is a cycling of dominance - a version of coexistence. One serotype has an outbreak wave while the other is present to a lesser degree, and after a time, the dominant serotype's presence lessens while the other grows until a switch in dominance takes place. Cycling of this nature was observed in Matlab, Bangladesh between 1983 and 2005 [7]. Similar behavior has been observed in Haiti following an outbreak in 2010, dubbed serotype switching instead of cycling due to the short timeframe of cholera presence [11]. We investigate which mechanisms drive the cycle dynamics and contribute to switches in dominance. Understanding these mechanisms will contribute to optimizing control strategies for outbreaks in host populations, such as those seen in [12,13].

* Corresponding author.
E-mail address: cameron.browne@louisiana.edu (C. Browne).
[1] Current address: Department of Mathematics, Virginia Tech, Blacksburg, VA, USA.

https://doi.org/10.1016/j.mbs.2023.109086
Received 10 May 2023; Received in revised form 3 October 2023; Accepted 5 October 2023
Available online 10 October 2023

Several factors are thought to be influential in creating cyclic behavior: serotypes have the same life-history traits [14]; induced cross-immunity between serotypes [14]; and seasonality (i.e. increase in infections due to a rainy season) [15]. Several papers have investigated these cycles with models built to incorporate both serotypes [7–9]. These studies showed that the oscillations observed depend strongly upon both seasonality and cross-immunity. The periodic relationship was explored via analysis of damped oscillations of the coexistence equilibrium of the autonomous system, observing that natural frequencies modulate the bifurcation structures of the forced system via the cross-immunity parameter. The seasonality incorporated into the model used by Kamo and Sasaki (and Adams and Boots) gave sustained oscillations for limited ranges of parameter values. However, these models did not consider the role of the environment in the transmission of the disease or serotype specific waning, so we incorporate these factors and build off the $SIRP$ model presented in [3].

In this paper, we examine the two serotype $SIRP$ model, considering the effect of seasonality by changing the environment-to-host transmission parameter to be a periodic function of time. We explore the initial autonomous model analytically and also perform numerical investigations of the system and with and without periodic forcing. The basic reproduction number (R_0) is established, with the disease-free equilibrium globally asymptotically stable when $R_0 \leq 1$. We show that there exists two unstable single-strain ("boundary") equilibria and a unique coexistence equilibrium when $R_0 > 1$. While the complexity of our derived coexistence equilibrium stifles proving convergence, we prove that the disease is uniformly persistent in the population. Furthermore, numerical simulations of the infectious host compartments of the autonomous system show damped, anti-phase oscillations which converge to equilibrium. Simulations of the corresponding non-autonomous system give undamped solutions while synchronizing the oscillations of the two solutions. The speed of synchronization depends on the degree of seasonality and cross-immunity present. We use simulations to further explore the effects of the seasonal forcing, cross-immunity, multiple transmission pathways, and the impact of coinfection (or lack thereof) on the periodicity and phase shift of solutions.

2. Model and analysis

Our model is similar to the classic SIR epidemic model, but we consider two cholera strains and add the extra compartments P_1 and P_2 to represent the concentrations of the pathogen strains in the environment. New individuals are born at a constant total rate μ, which is also the per-capita death rate. The susceptible hosts, S, can be infected by either strain, from a first-time infected host via $\beta_1 S I_j$, from a pathogens in the environment via $\delta S P_j$, or from a host with a re-infection at rate $\beta_2 S I_{jk}$. Infected individuals shed pathogens into the environment via rates $\alpha_1 I_j$ and $\alpha_2 I_{kj}$. We assume that the pathogen does not proliferate in the environment. First time and re-infected individuals, I_j and I_{kj}, respectively, recover at per-capita rates ν. Upon recovering from strain j, an individual can be reinfected with strain k at a reduced rate via $((1-\gamma)\beta_1 I_k + \beta_2 I_{jk})R_j$, where γ is the cross immunity parameter. Note that $\gamma = 1$ represents perfect cross immunity (i.e. recovered individuals from one strain cannot be infected with the other strain) while $\gamma = 0$ represents no cross immunity (i.e. recovered from one strain are fully susceptible to infection from the other strain). Additionally, we define a parameter $0 \leq \eta \leq 1$ to be the probability of gaining permanent immunity after re-infection. Previous models of two cholera serotypes have assumed permanent serotype specific immunity after infection so that there is full immunity after secondary infection with the distinct serotype from first infection. However, other models of cholera have that waning immunity and multiple re-infections are possible biologically. Thus, the parameter η generalizes the case of permanent immunity after secondary infection ($\eta = 1$) to allow for re-infection by the distinct serotype from most recent infection with probability $1-\eta$. Note that we assume there are no consecutive reinfections by the same strain, which we will explain further as we focus our analysis on the case $\eta = 0$ (no permanent immunity). For convenience, we list breif descriptions of the variables and parameters of our model in Table 1. Also, note that all proofs from model analysis to follow are located in Appendix A.

The resulting system, based off of the models in [3,7], is the following set of ordinary differential equations for $j, k = 1, 2,\ j \neq k$:

$$\begin{aligned}
\frac{dS}{dt} &= -\beta_1(I_1 + I_2)S - \beta_2(I_{12} + I_{21})S - \delta(P_1 + P_2)S + \mu(1 - S)\\
\frac{dI_j}{dt} &= \beta_1 I_j S + \beta_2 I_{kj} S + \delta P_j S - (\nu + \mu) I_j\\
\frac{dR_j}{dt} &= \nu I_j + (1-\eta)\nu I_{kj} - (1-\gamma)(\beta_1 I_k + \beta_2 I_{jk})R_j - (1-\gamma)\delta P_k R_j - \mu R_j\\
\frac{dI_{kj}}{dt} &= ((1-\gamma)(\beta_1 I_j + \beta_2 I_{kj}) + (1-\gamma)\delta P_j)R_k - (\eta\nu + (1-\eta)\nu + \mu) I_{kj}\\
\frac{dR_{kj}}{dt} &= \eta\nu I_{kj} - \mu R_{kj}\\
\frac{dP_j}{dt} &= \alpha_1 I_j + \alpha_2 I_{kj} - r_j P_j.
\end{aligned} \tag{2.1}$$

A schematic diagram of model (2.1) is presented in Fig. 1. Notice that since the R_{kj} component is decoupled, we can effectively ignore that component in our analysis. Also, note that the host population subsystem has been implicitly normalized, so $N := S + I_1 + I_2 + I_{12} + I_{21} + R_1 + R_2 + R_{12} + R_{21} \leq 1$. Indeed, by a standard argument, we have that this system is well-posed and dissipative (that is, for each non-negative initial condition, a unique solution exists which will always stay non-negative and is attracted to a bounded set). Solutions starting in the bounded set remain in there, i.e. the set is *positively invariant*, as detailed further in the following proposition:

Proposition 2.0.1. *System (2.1) is well-posed and dissipative in $\mathbb{R}^{11}_+$ and positively invariant on the set*

$$\begin{aligned}
\{x = (S, I_1, I_2, R_1, R_2, I_{21}, I_{12}, R_{21}, R_{12}, P_1, P_2) \in \mathbb{R}^{11}_+ |\\
N = S + I_1 + I_2 + R_1 + R_2 + I_{21} + I_{12} + R_{21} + R_{12} \leq 1,\\
P_1 + P_2 \leq \frac{A}{r}\},
\end{aligned} \tag{2.2}$$

where $A := \max\{\alpha, \alpha_2\}$, $r := \min\{r_1, r_2\}$. *Furthermore, since the birth and death rates are equal, the host population is conserved, and* $\{x \in \mathbb{R}^{11}_+ | N = 1\}$ *is an invariant set.*

Our model is tailored toward the two most prevalent serotypes of cholera, Ogawa and Inaba, which differ primarily in certain expressed antigens, leading to less immunity against the other serotype than against the most recent infecting serotype. Additionally, these serotypes are not thought to differ significantly in virulence or other life-history parameters [14]. Thus, we consider symmetric parameters with imperfect cross-immunity for the two serotypes in model (2.1). Also, an important complexity for cholera is seasonality, which will be considered later in this paper, and is the driving force behind the sustained cycling found in prior serotype models [7–9] (see Fig. 1).

Our system contains a few key differences between the previous serotype models in [7–9]. First, as noted before, we add the environmental pathogen component, which is the major transmission route for cholera. Next, underlying the construction of a simplified model detailed in [7–9] is the assumption that one can be infected with both strains simultaneously, which we do not assume in our model. Although there are examples of pathogens where coinfection is observed (e.g. HIV and HBV), to the best of our knowledge, there is no documented evidence of coinfection with distinct cholera serotypes, and phylogenetic studies have concluded that within-patient mutation was a more likely source of variation than coinfection with multiple strains of V. cholerae [16]. There are several reasons for rarity of

Table 1
Variables and parameters with units for the model.

S	Susceptible population density	unitless
I_j	Density of strain j infectious individuals	unitless
I_{kj}	Density of individuals previously infected with strain k, currently infected with strain j	unitless
R_j	Density of strain j recovered population	unitless
R_{kj}	Density of population recovered from strain k and strain j	unitless
P_j	Strain j bacteria population in the environment	cells
μ	Host population turnover rate (birth rate = death rate)	1/day
β_1	Transmission rate from 1st time infected host	1/day
β_2	Transmission rate from reinfected host	1/day
δ	Environment-to-host transmission rate	1/(cells × day)
ν	Recovery rate	1/day
γ	Cross-immunity factor	$\gamma \in [0,1]$
η	Probability of gaining permanent immunity after reinfection	$\eta \in [0,1]$
α_1	Pathogen shedding rate into environment from 1st time infected host	cells/(day × individual)
α_2	Pathogen shedding rate into environment from reinfected host	
r	Pathogen decay rate	cells/(day × individual)

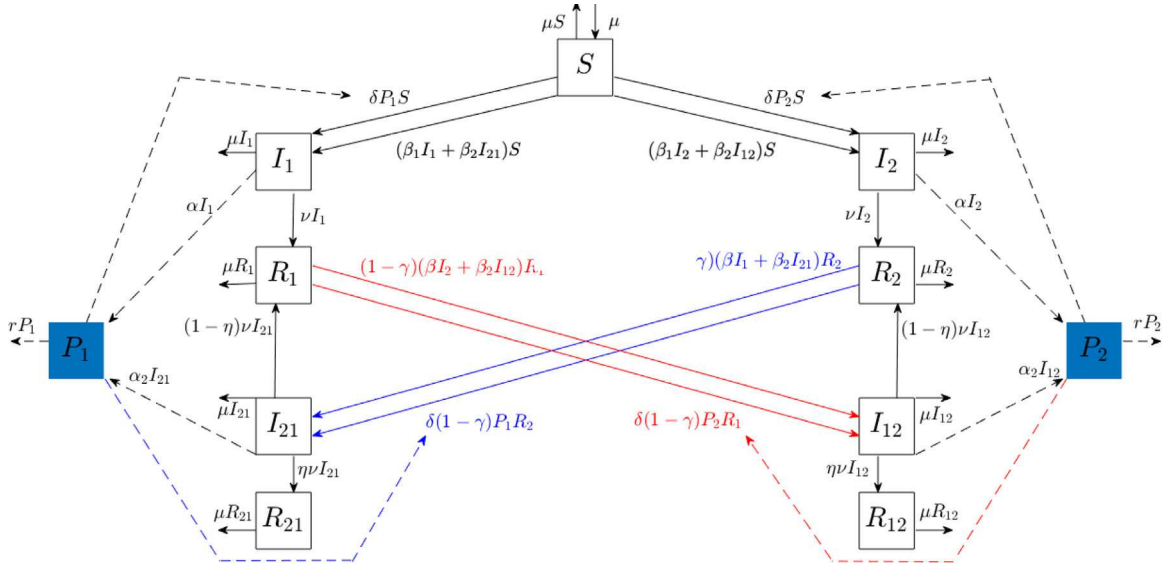

Fig. 1. Schematic diagram of (2.1). Solid lines represent dynamics of host densities. Dashed lines represent dynamics of pathogen population. Red and blue lines signify secondary infections from strains 1 and 2, respectively.

coinfection: low probability of distinct exposures, especially if serotype prevalence cycles; within-host competition negatively impacting overall infection as observed with dengue serotypes [17]; or interference of second infection through immune stimulation by initial infecting strain, which has been observed between the rhinovirus and the influenza A virus [18]. Thus, we focus on the case when coinfection does not occur although we do briefly consider coinfection in Section 3.2 to have a more complete comparison of results with prior works. Finally, we allow for susceptibility to sequential re-infections by distinct serotype from previous infection with probability $1-\eta$, as opposed to assuming lifelong serotype-specific immunity.

Now, we consider the case $\eta = 0$, along with $\beta := \beta_1 = \beta_2$, $\alpha := \alpha_1 = \alpha_2$, which reduces the system to

$$\begin{aligned}
\frac{\mathrm{d}S}{\mathrm{d}t} &= -\beta(y_1+y_2)S - \delta(P_1+P_2)S + \mu(1-S)\\
\frac{\mathrm{d}y_j}{\mathrm{d}t} &= \beta y_j S + \delta P_j S + (1-\gamma)\beta y_j R_k + (1-\gamma)\delta P_j R_k - (\nu+\mu)y_j\\
\frac{\mathrm{d}R_j}{\mathrm{d}t} &= \nu y_j - (1-\gamma)\beta y_k R_j - (1-\gamma)\delta P_k R_j - \mu R_j\\
\frac{\mathrm{d}P_j}{\mathrm{d}t} &= \alpha y_j - r P_j,
\end{aligned} \tag{2.3}$$

where $y_j = I_j + I_{kj}$ is the total density of individuals infected with strain j.

We consider (2.3), a special case of the more general system (2.1), as a model of serotype cycling with environmental transmission. An implicit assumption in the above model is that immunity gained by recovery from one serotype is lost after infection from the other serotype (i.e. by reentering compartment R_j after exiting compartment I_{kj}). This consideration allows us to reduce the number of equations for the model, as in the prior serotype models [7–9] while still allowing more than two sequential individual infections (alternating between serotypes). Studies have shown that the mean time between heterologous infections is much lower than the mean time between homologous infections, and cross-immunity against the other strain is weaker than immunity against the infecting strain [19]. Essentially, while reinfections from the same strain are not common [7], immunity does wane over time, and reinfection is possible [19]. Our minimal model considers the more typical case of secondary infection with a different serotype than the previous infection (heterologous sequential infections). The model considers serotype cycling on an individual level and explores if that drives serotype cycling on the level of the population.

By Proposition 2.0.1, system (2.3) is well-posed and dissipative in $\mathbb{R}^7_+$ and positively invariant on the set

$$\mathcal{A} = \{(S, y_1, y_2, R_1, R_2, P_1, P_2) \in \mathbb{R}^7_+ | S+y_1+y_2+R_1+R_2 \leq 1,\ P_1+P_2 \leq \frac{\alpha}{r}\}. \tag{2.4}$$

We use $\mathring{\mathcal{A}}$ to denote the interior of $\mathcal{A}$.

2.0.1. Disease free equilibrium

Notice that at the disease free equilibrium (DFE), $(\bar{S}_0, 0, 0, 0, 0, 0)$, $\bar{S}_0 = 1$ since the population is normalized. We use the next generation method as shown in [3,20] to characterize its stability.

We define a next-generation matrix by considering the linearized system at the DFE. We divide the population into non-infected individuals, consisting of susceptible and recovered compartments, and infected states with the remaining variables. Then the linearized "infection" subsystem is $\mathbf{x}' = (F - V)\mathbf{x}$, where $\mathbf{x} = (y_1, y_2, P_1, P_2)$, F contains entries corresponding to new infections, and $-V$ contains all other transition terms in the Jacobian matrix evaluated at $\mathcal{E}_0$:

$$F = \begin{pmatrix} \beta & 0 & \delta & 0 \\ 0 & \beta & 0 & \delta \\ 0 & 0 & 0 & 0 \\ 0 & 0 & 0 & 0 \end{pmatrix}, \quad V = \begin{pmatrix} (\nu+\mu) & 0 & 0 & 0 \\ 0 & (\nu+\mu) & 0 & 0 \\ -\alpha & 0 & r & 0 \\ 0 & -\alpha & 0 & r \end{pmatrix}. \tag{2.5}$$

Notice

$$FV^{-1} = \begin{pmatrix} \frac{\beta}{\nu+\mu} + \frac{\delta\alpha}{r(\mu+\nu)} & 0 & \frac{\delta}{r} & 0 \\ 0 & \frac{\beta}{\nu+\mu} + \frac{\delta\alpha}{r(\mu+\nu)} & 0 & \frac{\delta}{r} \\ 0 & 0 & 0 & 0 \\ 0 & 0 & 0 & 0 \end{pmatrix}. \tag{2.6}$$

The basic reproduction number for this system is the spectral radius of FV^{-1},

$$R_0 = \frac{\beta}{(\nu+\mu)} + \frac{\delta}{(\nu+\mu)}\left(\frac{\alpha}{r}\right). \tag{2.7}$$

The first term represents the average number of secondary infections from one infectious individual during its infectious period through host-to-host transmission; the first factor in the second term represents the same with respect to environment-to-host transmission, regulated by the second factor with respect to pathogen shedding and decay. The first diagonal entry represents the basic reproduction number of strain 1 when considering it in a single-strain $SIRP$ model; the second would represent the same for strain 2 in a single strain $SIRP$ model.

Standard analysis allows us to conclude that the DFE is locally asymptotically stable on $\mathcal{A}$ for $R_0 < 1$. We extend this further to global stability in the following result.

Theorem 2.1. *If $R_0 \leq 1$, then the DFE is globally asymptotically stable in $\mathcal{A}$.*

The proof in Appendix A uses the method introduced by [21] of constructing a Lyapunov function from the next generation method decomposition. Note that for a periodic version of the model with seasonality introduced in Section 3, we also prove that the DFE is globally attracting when the corresponding periodically defined R_0 is strictly less than one (see Appendix C).

2.0.2. Single-strain equilibria

Biologically, single-strain equilibria represent the possibility of competitive exclusion — one strain maintains a nonzero steady state while the other strain is driven to extinction with all relevant compartments resting at zero. Specifically, at the strain j single-strain equilibrium (SSE), E_j, the strain k components are zero. Thus, E_j can be considered as the strain k DFE with components

$$\begin{aligned} \bar{S}_j &= \frac{r(\mu+\nu)}{\beta r + \alpha\delta} = \frac{1}{R_0} \\ \bar{y}_j &= \frac{\mu(\beta r + \alpha\delta - r(\mu+\nu))}{(\nu+\mu)(\beta r+\alpha\delta)} = \frac{\mu r}{\beta r+\alpha\delta}(R_0 - 1) \\ \bar{R}_j &= \frac{\nu}{\mu}\bar{y}_j = \frac{\nu r}{\beta r+\alpha\delta}(R_0-1) \\ \bar{P}_j &= \frac{\alpha}{r}\bar{y}_j = \frac{\alpha\mu}{\beta r+\alpha\delta}(R_0-1) \end{aligned} \tag{2.8}$$

and $y_k = R_k = P_k = 0$. Hence, for $R_0 > 1$, both single-strain equilibria are nonnegative with invasion fitness number (the "basic reproduction number" when viewing this equilibrium as a strain k DFE)

$$R^{(k)}_{inv} = \rho(FV^{-1}) = 1 + (1-\gamma)\frac{\nu}{\nu+\mu}(R_0 - 1) \tag{2.9}$$

where

$$F = \begin{pmatrix} \beta\bar{S}_j + (1-\gamma)\beta\bar{R}_k & \delta\bar{S}_j + (1-\gamma)\delta\bar{R}_k \\ 0 & 0 \end{pmatrix} = \left(\frac{1}{R_0} + (1-\gamma)\bar{R}_k\right)\begin{pmatrix} \beta & \delta \\ 0 & 0 \end{pmatrix}$$

and

$$V = \begin{pmatrix} \nu+\mu & 0 \\ -\alpha & r \end{pmatrix}.$$

Symmetry of parameters allow us to conclude that $R^{(j)}_{inv} = R^{(k)}_{inv} := R_{inv}$. Note that the invasion reproduction numbers depend on cross-immunity γ - the smaller the degree of cross-immunity, the stronger the force of infection from each strain. Threshold dependence of invasion reproduction numbers is on R_0, though, which leads to instability of the single-strain equilibria.

Lemma 2.2. *Both single-strain equilibria E_1 and E_2 exist if and only if $R_0 > 1$. When they exist, they are unstable.*

This result is consistent with the biological observation in Bangladesh that competitive exclusion between the serotype strains does not occur [7]. However, within its boundary — that is, when S, y_j, R_j, and P_j are initially nonzero, and $y_k = R_k = P_k = 0$ - the strain j singe-strain equilibrium is globally asymptotically stable. Formally, we define the boundary sets:

$$\begin{aligned} X^{(1)}_0 &= \{(S, y_1, 0, R_1, R_2, P_1, 0) \in \mathbb{R}^7_+ | y_1 + P_1 > 0\}, \\ X^{(2)}_0 &= \{(S, 0, y_2, R_1, R_2, 0, P_2) \in \mathbb{R}^7_+ | y_2 + P_2 > 0\}. \end{aligned} \tag{2.10}$$

Theorem 2.3. *The strain j single-strain equilibrium is globally asymptotically stable within the strain j boundary $X^{(j)}_0$ if $R_0 > 1$.*

2.0.3. Coexistence equilibrium

The result that both single-strain equilibria will be unstable if they exist is a strong indication of a coexistence result, either in the form of a periodic solution (more likely a result for the forced system explored later and is consistent with biological observations in [7]) or coexistence equilibrium. We can prove several results about positive equilibria depending on the magnitude of γ. The first result below supports intuitive understanding of coexistence equilibria for a system with symmetric parameters and provides a simplification useful for proving Proposition 2.4.1.

Lemma 2.4. *Given the existence of a coexistence equilibrium $(\bar{S}, \bar{y}_1, \bar{y}_2, \bar{R}_1, \bar{R}_2, \bar{P}_1, \bar{P}_2)$ of the serotype system with symmetric parameters, it follows that $\bar{y}_1 = \bar{y}_2$, $\bar{R}_1 = \bar{R}_2$, and $\bar{P}_1 = \bar{P}_2$.*

Hence, we can write the coexistence equilibrium as $(\bar{S}, \bar{y}, \bar{y}, \bar{R}, \bar{R}, \bar{P}, \bar{P})$. Solving, we obtain two possible nontrivial solutions for the system (details included in Appendix B). The terms for the two possible coexistence equilibria $(\bar{S}, \bar{y}, \bar{y}, \bar{R}, \bar{R}, \bar{P}, \bar{P})$ are written out below.

Table 2
System (2.3) equilibria and stability.

Equilibria	Existence	Stability
$E_0 = (1, 0, 0, 0, 0, 0, 0)$	always exists	GAS if $R_0 \leq 1$; unstable if $R_0 > 1$
$E_1 = (\frac{1}{R_0}, \frac{\mu r}{B}(R_0 - 1), 0, \frac{\nu r}{B}(R_0 - 1), 0, \frac{\alpha\mu}{B}(R_0 - 1), 0)$	exists iff $R_0 > 1$;	always unstable
$E_2 = (\frac{1}{R_0}, 0, \frac{\mu r}{B}(R_0 - 1), 0, \frac{\nu r}{B}(R_0 - 1), 0, \frac{\alpha\mu}{B}(R_0 - 1))$	exists iff $R_0 > 1$	always unstable
$E_3 = (S_+, y_+, y_+, R_+, R_+, P_+, P_+)$	exists if $R_0 > 1$ and $0 < \gamma < 1$	stability unknown

$$\begin{aligned}
\bar{S}_\pm &= \frac{-\sigma(B + \mu r) + 2Ur \pm Q}{2B(2 - \sigma)} \\
&= \frac{\mu r}{\mu r + 2B\bar{y}_\pm} \\
\bar{y}_\pm &= \frac{\sigma(B - \mu r) - 2Ur \pm Q}{4B\sigma} \\
\bar{R}_\pm &= \frac{\nu r \bar{y}_\pm}{\mu r + \sigma B \bar{y}_\pm} \\
\bar{P}_\pm &= \frac{\alpha}{r}\bar{y}_\pm
\end{aligned} \tag{2.11}$$

where

$B := \beta r + \alpha\delta,\ \sigma := 1 - \gamma,\ U := \mu + \nu,$ and

$Q = \sqrt{(2Ur - \sigma(B + \mu r))^2 + 4\sigma B\mu r(2 - \sigma)}.$

The following proposition establishes existence and uniqueness of the coexistence equilibrium.

Proposition 2.4.1. *If $R_0 > 1$ and $0 < \gamma < 1$, then there exists a unique coexistence equilibrium given by $(\bar{S}_+, \bar{y}_+, \bar{y}_+, \bar{R}_+, \bar{R}_+, \bar{P}_+, \bar{P}_+)$ in (2.11).*

Notice that if $\gamma = 1$ and $R_0 > 1$, then there exists a line of coexistence equilibria defined by the equation $\frac{f(S)}{S} = -(\beta + \frac{\delta\alpha}{r})(y_1 + y_2)$ with $f(S) = \mu(1 - S)$. The Jacobian of the resulting system evaluated at a coexistence equilibrium has an eigenvalue $\lambda = 0$ (see Appendix B). The behavior of the solutions around this set remains an open problem, but we suspect the set of equilibria is stable and attracting.

We summarize the findings regarding our equilibria in Table 2.

2.1. Disease persistence

The previous section displayed the global asymptotic stability of the DFE when $R_0 \leq 1$ and the existence of a unique coexistence equilibrium. The structure of the coexistence equilibrium makes statements about its stability elusive, but we can obtain uniform persistence for the system. All relevant definitions are located in Appendix A.

Theorem 2.5. *Let $R_0 > 1$ for system (2.3). Then, both strains of the disease uniformly persist in $\mathbb{R}^7_+$; that is, there exists an $\epsilon > 0$ such that if $\min\{y_1(0) + P_1(0), y_2(0) + P_2(0)\} > 0$, then*

$$\liminf_{t\to\infty} \min\{y_1(t), P_1(t), y_2(t), P_2(t)\} > \epsilon.$$

The uniform persistence tells us that both strains of the disease will persist over time in the population. Graphically, they will move away from the competitive exclusion equilibria towards the coexistence equilibrium as long as $R_0 > 1$. For practical purposes like determining control measures (e.g. vaccination strategies), this result is too vague; we need a more precise vision of how the disease will behave over time when it is endemic in a population. Further analytical results for the behavior of the system are difficult to obtain, so we turn to numerical simulations to explore coexistence dynamics.

3. Numerical exploration: stability, seasonal forcing and coinfection

A primary motivation of our study is on the serotype cycling behavior exhibited in Bangladesh, where data exhibits the behavior of the strains cycling (i.e. switching in dominance) in an undamped and anti-phase pattern [7]. In order to explore the possibility of serotype cycling in our system, we first numerically calculate stability of the derived coexistence equilibrium (since analytical formulation was not feasible). As in [7,8], simulations show damped oscillations eventually converging to the coexistence equilibrium corresponding to the presence of complex eigenvalues with negative real part. In each simulation, we computed the eigenvalues and eigenvectors of the linearized system around the formulated coexistence equilibrium value, which indicated local asymptotic stability in all cases except $\gamma = 1$. Competitive exclusion is not exhibited.

We demonstrate numerically the effect that cross-immunity has on oscillatory behavior of solutions. We include one example of exploring the eigenvector relationship with oscillatory behavior as explored in [8] in Fig. 2(c) (expounded on later). We see the eigenvector components lying "opposite" each other corresponds to the anti-phase behavior seen in the autonomous model prior to convergence to equilibrium. Depending on γ, Kamo & Sasaki observe in-phase, damped solutions to their autonomous system — we generally see anti-phase, damped solutions (Fig. 2(a)). However, to capture similar dynamics to those observed in Bangladesh, we adjust our model to allow the possibility of undamped oscillatory behavior by introducing a periodic forcing function representing the effect of seasonality on environment-to-host transmission.

Cholera is known to depend heavily on seasons: outbreaks of cholera are significantly more prevalent during an area's rainy season [15,22]. One would then expect oscillations in the levels of infections — low levels of infection during a dry season and high levels of infection during the rainy season [23] - suggesting the presence of periodic solutions. Additionally, as observed in Bangladesh, data collected over a period of about 20 years not only displayed the expected oscillatory behavior but also showed regular switches in dominance between the two observed serotypes, Ogawa and Inaba [7], i.e. the presence of stable, quasiperiodic, anti-phase cycles for the two infectious host populations. We attempt to qualitatively match this data and reproduce the behavior by introducing a seasonal change in transmission rate. We rewrite the environment-to-host transmission rate δ as

$$\delta_t = \delta(1 + \delta_0 \sin(2\pi t/365.2242)) \tag{3.1}$$

where δ is now the base transmission rate and $\delta_0 \in [0, 1]$ measures the degree of seasonality. The forcing function creates a non-autonomous system to which much of the previous analysis does not apply. However, we are able to construct the basic reproduction number R_0 for the periodic system and prove global asymptotic stability of the DFE of the non-autonomous system when $R_0 < 1$, presented in Appendix C.

The periodic forcing creates sustained oscillations and eventually synchronizes the transient anti-phase dynamics; however, the length of the transient serotype cycling depends upon cross-immunity γ, for which we refer to previous work to better understand the mechanisms behind this behavior. Kamo & Sasaki (2002) use the explicit expression for their coexistence equilibrium to show that the natural frequency associated with anti-phase oscillations at this equilibrium is dependent on both cross-immunity σ ($\sigma := 1 - \gamma$) and transmission β, while the natural frequency associated with the in-phase oscillations is dependent only upon cross-immunity. They conclude that the smaller σ is, the more the anti-phase mode contributes to solution behavior, allowing an indication of which mode to expect influencing the behavior of the solution [8,9]. Note that β, the host-to-host transmission rate, is

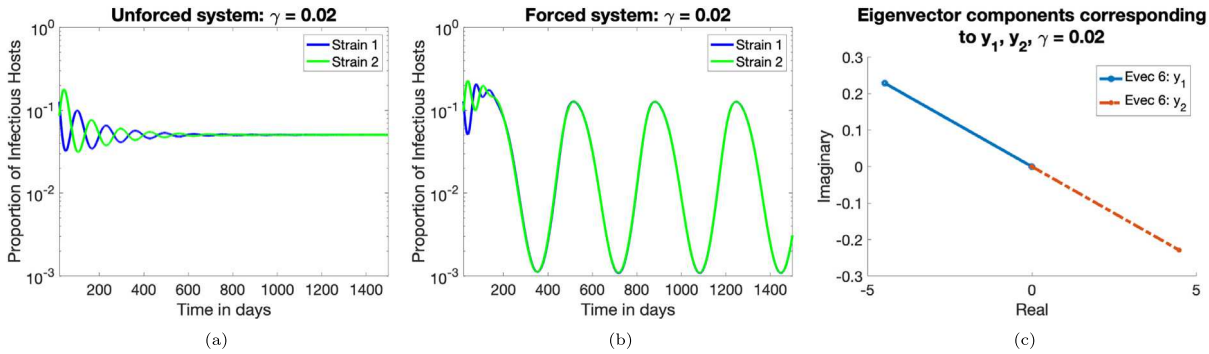

Fig. 2. Eigenvector influence on system (2.3) oscillations. 2(a): The eigenvalues of the Jacobian all have negative real part, confirming our observation that the proportion of host populations converge to the equilibrium value of 0.0549. 2(b): The forcing function takes the damped, anti-phase oscillations in the autonomous system and synchronizes them to an in-phase periodic solution. The disease does not die out in the graph of the forced system although the minimums do get close to 0. Note that the dynamics of the pathogen populations for large enough time will be the same as those of the host population since the pathogen solution becomes proportional to the host solution as t increases. 2(c) We graph the second and third components of the eigenvector (those corresponding to strain 1 and strain 2 infectious hosts, respectively) corresponding to the pair of complex conjugate eigenvalues in the manner of [8]. The eigenvectors are "opposites", indicating the presence of the anti-phase behavior we see at the beginning of both solutions. This simulation produced only one pair of complex eigenvalues, so we do not have a second pair of eigenvectors to represent the "in-phase" oscillations as in [8].

transformed by the seasonal forcing function in their model, whereas we write the environment-to-host transmission rate, δ, as our parameter affected by seasonal forcing. It follows that the natural frequency will be affected when forces of transmission β or δ are affected by the forcing function. Extending these results of both cross-immunity and transmission influences, Adams & Boots (2007) conclude that solutions with in-phase dynamics are more common than those with anti-phase dynamics [9]. We were not able to derive this same approximation due to additional complexities in our system, but our model behavior agrees with the results for their systems. Figs. 3 and 4 give patterns of oscillatory behavior changing with respect to γ, where changes in γ affect the "period" (i.e. time between peaks), speed of convergence, and amplitudes. Thus, the intensity of cross-immunity is observed to affect how often a serotype switch in dominance occurs, how quickly a stable steady state (without seasonal forcing) or in-phase periodic solution (with seasonal forcing) is reached, and the total case load for both strains.

We simulate the solutions of the proportion of infectious hosts and compare the unforced system (2.3) and its forced system. Parameters (see Table 3) from [3,7] are adjusted to account for the normalization of the model and the time scale given in days. Log-scale on the y-axis is used for ease of comparison between figures. Sustained, anti-phase periodic solution remain elusive, except in a resonant case around $\gamma = 0.4$ discussed below. All other simulations using the forcing function for the consolidated model lead to final convergence to in-phase solutions. However, in some simulations, the forcing function provides the necessary change in the system to exhibit behavior very similar to that seen in the Bangladesh data: an anti-phase, undamped periodic solution for a long period of time prior to convergence to in-phase solutions. For biological purposes, this period of time could be considered "long enough" in the host population time scale to consider the solution as having sustained anti-phase oscillations.

Simulations for the autonomous and non-autonomous systems exhibited anti-phase behavior similar to that in the Bangladesh dataset for an approximate range of $0.4 \leq \gamma \leq 0.8$ (Figs. 3, 4). As cross-immunity strengthens, competitive behavior increased between the two strains. The forced system in particular displays rapid interannual cycles [7] for some values of γ in this range — seasonal forcing creates rapid fluctuations in case loads for each strain. The autonomous system displays a moderate amount of these cycles for $\gamma \approx 0.8$ and gives higher amplitude damped solutions for an approximate range of $0.4 \leq \gamma \leq 1$. The behaviors of the two systems show the most disparity approaching $\gamma = 0.5$ from either direction but grow in similarity as γ approaches 0 and 1, with anti-phase cycles synchronizing in amplitude and period, and with inter-annual cycles dampening in the case of Fig. 3. In the case of Fig. 3, solutions are nearly indistinguishable between the two systems for high values of γ. Environment-to-host transmission δ is small and the degree of seasonality δ_0 is low, and the influence of cross-immunity outcompetes the low influence of seasonal forcing as γ increases, synchronizing the systems' behaviors. Thus, strong cross-immunity between strains can outweigh the effects of weak seasonal forcing in disease dynamics. Section 3.1 further explores the effects of seasonal forcing on transmission. Out-of-phase (that is, neither in-phase nor anti-phase) oscillations appear for $\gamma > 0.5$ in Fig. 3 .

A threshold for γ appears around 0.4 (Figs. 3, 4) where the non-autonomous solutions switch from fast synchronization to long-term transient cycling. Around this threshold, Fig. 4 shows resonance appearing in the solution to the non-autonomous system. Further investigation shows this anti-phase resonance occurring for an approximate range of $0.395 \leq \gamma \leq 0.4125$. These irregular oscillations eventually settle into sustained anti-phase oscillations with "pulses", where minor anti-phase small amplitude waves (pulses) occur in-phase with major larger amplitude anti-phase oscillations (see Fig. 5). For $\gamma > 0.4125$, convergence to in-phase oscillations occurs once again although convergence occurs more slowly than for $\gamma < 0.395$. Adams & Boots found similar longer period resonant behavior in their system for a similar range of γ, $(0.35 < \gamma < 0.4)$ [9]. Summaries of results from past studies and comparisons of numerical results for both the autonomous and non-autonomous models from system (2.3) can be found in Tables D.4 and D.5 in Appendix D.

We note behavior of the special cases of the system when $\gamma = 0$ and 1. When $\gamma = 0$, the two strains can behave almost independently from one another since they can freely infect any host regardless of prior infections [8]. Notice that in the simulations shown in the two examples above, the solutions converge to the same behavior over time in both the forced and unforced systems. When $\gamma = 1$, the system can be written as

$$\begin{aligned}
\frac{dS}{dt} &= \mu(1-S) - (\beta y_1 + \delta P_1)S - (\beta y_2 + \delta P_2)S \\
\frac{dy_j}{dt} &= (\beta y_j + \delta P_j)S - (\nu + \mu)y_j \\
\frac{dR_j}{dt} &= \nu y_j - \mu R_j \\
\frac{dP_j}{dt} &= \alpha y_j - r P_j.
\end{aligned} \tag{3.2}$$

Table 3
Parameter values, R_0, and initial conditions in simulations.

Parameter	Fig. 2	Fig. 3	Fig. 4	Fig. 6	Figs. 7, 8
β	0.125	0.30547 [7]	0.13576	ranges wrt R_0, δ	see Fig. 3
δ	0.5	1.07×10^{-7} [3]	1.804×10^{-6}	ranges wrt R_0, β	see Fig. 3
μ	4.978×10^{-5}	7.056×10^{-5} [7]	see Fig. 3	see Fig. 3	see Fig. 3
ν	1/9.5	1/9.5 [7]	see Fig. 3	see Fig. 3	see Fig. 3
α	1/5	10^6 [3]	see Fig. 3	see Fig. 3	10^8
r	0.9	10 [3]	see Fig. 3	see Fig. 3	see Fig. 3
δ_0	0.9	0.1	see Fig. 3	see Fig. 3	0.15
γ	0.02	ranges over [0, 1]		see Fig. 3	0.5
R_0	2.2420	3.0016	see Fig. 3	see Fig. 3	13.0582

Note that values without references are assumed values used in simulations.

As mentioned in Section 2.0.3, this yields a line of coexistence equilibria, which may be a stable attracting set. This has yet to be proven, but simulations support this claim. Perfect cross-immunity makes the strains biologically indistinguishable; if infected densities are combined, the system ought to act as a single strain model (with densities half the size) [8]. Simulations support this, showing that the strain with the largest initial condition will dominate the other strain and remain dominant in a manner of coexistence — both strains remain present in the population and follow the same pattern of behavior. Solutions to the autonomous system can converge to two distinct equilibria values, and solutions to the non-autonomous system will oscillate together in the same manner, with one always larger than the other.

3.1. Comparing transmission pathways

System (2.3) considers multiple transmission pathways: infections occur from hosts interacting with infectious hosts as well as from hosts interacting with the contaminated environment. Both are important pathways to consider [24]. At the peak of an outbreak, host-to-host transmission contributes significantly to infections, and it is suggested that this contributes to the rapid spread of the disease, while environmental transmission drives slower dynamics [25]. To compare the dual infection routes, we fix $R_0 = 3.0016$ as in Fig. 3 with $\gamma = 0.5$ and vary direct and environmental transmission parameters β and δ, ranging β from 0 to 0.3055 δ accordingly with respect to the fixed R_0. Fig. 6 shows that changing those transmission parameters has virtually no effect on the autonomous system dynamics, but in the non-autonomous system, increasing β and decreasing δ eventually slows the rate of synchronization of the solutions, increases the length of time between peaks, and changes the inter-cycle dynamics. Additionally, the overall case load amplitude decreases significantly, agreeing with the model's structure since the seasonal forcing is only linked to the environmental transmission mode. When δ is smallest, the oscillatory behavior is almost identical to that in the corresponding graph of the autonomous system, while the middle values of δ show less change in the rate of synchronization and exhibit oscillations that dampen more slowly, and large values of δ can provide more rapid synchronization with less dampening. In contrast, the smallest values of δ show significantly damped oscillations. Thus, with the inclusion of seasonality, we can conclude a strong dependence of the system's oscillatory behavior on transmission as well as on cross-immunity. Understanding oscillatory dynamics will inform of when a switch in serotype dominance is approaching and which serotype to vaccinate against, providing timely and cost-effective control against upcoming outbreaks.

3.2. Considering coinfection

Our simulations have only produced undamped, anti-phase oscillatory behavior for solutions to the infectious compartments in a particular resonant case (around $\gamma = 0.4$ as shown in Fig. 3), as opposed to larger parameter ranges showing cycling for the other models in [7,8], and [9], which consider an additional compartment to represent coinfection of both strains. We can incorporate a coinfection compartment I into System (2.1) in the same manner by assuming $\beta := \beta_1 = \beta_2$, $\alpha := \alpha_1 = \alpha_2$ (that is, transmission rate and shedding rate are the same for first and secondary infections), and considering $R := R_{12} + R_{21}$. If we consider permanent immunity after infection from both strains (i.e. take $\eta = 1$), then we can obtain their system (see below) with the addition of the pathogen compartments, dropping the R equation since it does not affect solution dynamics for the rest of the system. Since pathogen dynamics occur on a much more rapid time scale than those of the host, we apply quasi-steady state analysis and consider a time scale τ where $t = \epsilon\tau$; τ represents the fast time scale of the pathogen (e.g. decay rate) and t the slow time scale of the host (e.g. host life span). Then, we can consider host populations fixed with respect to the pathogen populations on the new time scale and solve the equation

$$0 = \alpha y_j - r P_j^*$$

to obtain a quasi-steady state P_j^* as a function of y_j: $P_j^*(y_j) = \frac{\alpha}{r} y_j$. Redefining $\beta := \beta + \frac{\delta\alpha}{r}$, the system then becomes that as considered in [7,8], and [9]:

$$\begin{aligned} \frac{dS}{dt} &= -\beta(y_1 + y_2)S + \mu(1 - S) \\ \frac{dy_j}{dt} &= \beta(S + (1-\gamma)z_k)y_j - (\mu + \gamma)y_j \\ \frac{dz_j}{dt} &= \beta S y_j + \beta(1-\gamma)z_j y_k - \mu z_k, \end{aligned} \tag{3.3}$$

where $y_j = I_j + I + I_{kj}$ represents the density of hosts infected by strain j and $z_j = I_j + R_j$ represents the density of hosts exposed to strain j but susceptible to strain k.

Note that when $\eta = 0$, the system does not consolidate when we have coinfection, contrary to system (2.3), so we do not explore the dynamics of the system with coinfection and $\eta = 0$. The z_j compartment plays a similar role to the R_j compartment in system (2.3), with the key difference being the first term of the differential equation. In system (3.3), the first term of $\frac{dz_j}{dt}$ is nonlinear, representing the rate of infection of susceptible individuals with strain j. The first term of $\frac{dR_j}{dt}$ in system (2.3), νy_j, represents the rate of recovery of infectious individuals. This difference in linearity appears to strongly affect the periodic and anti-phase behavior of the solutions. In most numerical simulations of system (2.3), we observe transient anti-phase dynamics (often with semi-chaotic oscillations) prior to convergence to an in-phase solution of the same period as the forcing function. Without the nonlinear term, system (2.3) does not have as much resonance to perturb the solution away from the general structure provided by the periodic forcing function. The nonlinearity seems to induce more resonance for creating periodic solutions with sustained anti-phase oscillations.

Fig. 7 displays simulations of the coinfection model with additional pathogen environmental compartment (no QSSA). Solutions exhibit undamped, anti-phase oscillations between serotypes, similar to the undamped, anti-phase cycling in serotype dominance in the Bangladesh data from [7]. We examine the behavior of the periodic solution as γ ranges between 0 and 1. Solutions appear out-of-phase when $\gamma = 0$, with the magnitude of strain 2 peaks greater than those of strain 1.

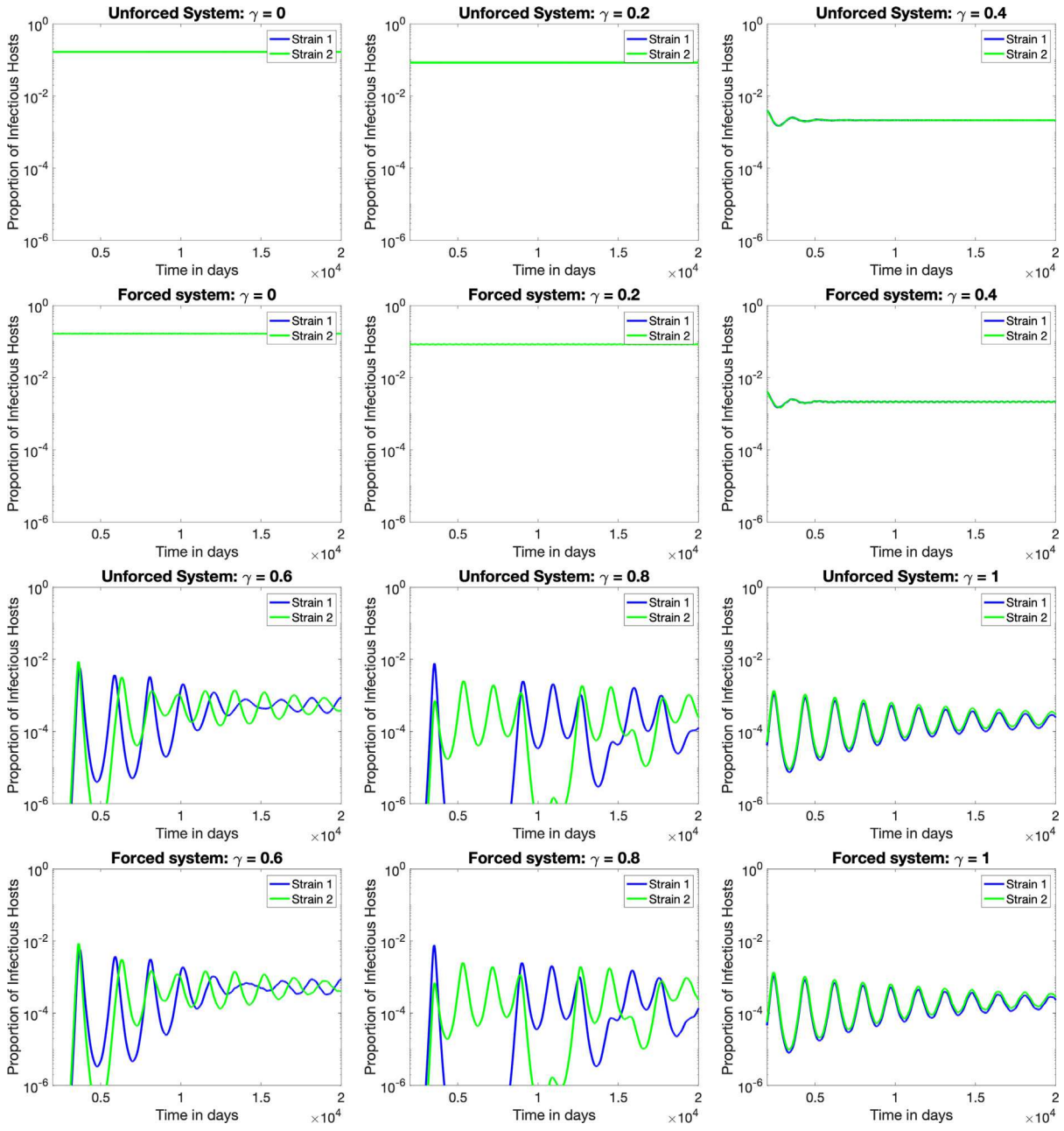

Fig. 3. Simulation of system (2.3). Eigenvalues of the Jacobian indicate the autonomous system solutions will be stable for $\gamma < 1$. Stability is inconclusive when $\gamma = 1$. All solutions exhibit some initial anti-phase oscillatory behavior, which resolve quickly when $\gamma < 0.5$, converging to the stable equilibrium value for the autonomous system and to in-phase oscillations for the non-autonomous system. The equilibria, maxima, and minima decrease as γ increases. Solution amplitudes increases as γ increases. The time between peaks for a single strain is about one year for $\gamma > 0.5$.

For weak cross-immunity $\gamma \approx 0.3$, solutions converge to anti-phase periodic solutions. Rapid fluctuations appear as behavior appears as γ approaches that critical threshold of 0.5, and anti-phase behavior reappears as cross-immunity continues to strengthen. For $\gamma = 1$, the solutions have in-phase interannual cycles, with strain 2 peaks of greater magnitude than those of strain 1. The amplitudes of both solutions decrease as γ approaches 1. The periods do not appear to have a monotonic dependency on γ as the period for $\gamma = 0.3$ is much shorter than for the other stable periodic solutions of γ.

Solutions of the autonomous system with these parameters (Fig. 8) display the expected anti-phase cycles converging to coexistence equilibrium. Interannual cycles appear for $\gamma > 0.5$ as similarly observed in the simulation of the autonomous system with coinfection component in [7]. For the smallest values of γ, the cycles are out-of-phase until convergence, and the phases separate further as γ increases. All other solutions settle into damped, anti-phase oscillations that converge to the equilibrium; any interannual cycles disappear. When $\gamma = 1$, solutions oscillate in-phase with strain 2 always having larger magnitude than strain 1. The periods for these solutions vary; notice the increase when $\gamma = 0.5$ and $\gamma = 0.8$, where the period increases from 1 year to 2–3 years. We conclude that the inclusion of coinfection gives a larger range of parameter values for cycling with higher amplitude resonant anti-phase periodic solutions. However, we do find transient anti-phase oscillations for long enough times to match cycling observed in Bangladesh for γ between 0.4 and 0.8 in our forced model without coinfection. Furthermore, the autonomous system always displayed

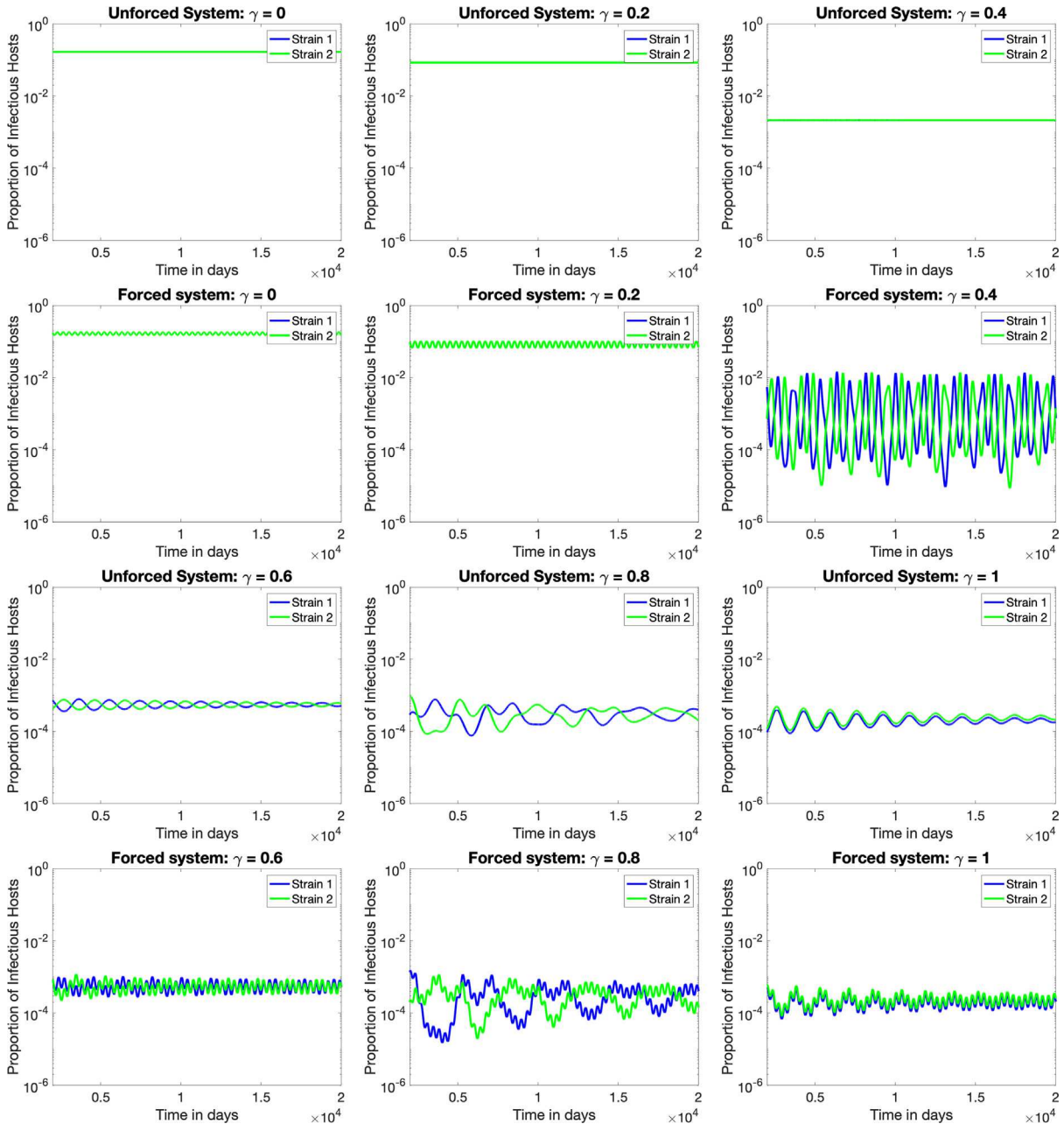

Fig. 4. Simulation of system (2.3). Parameters, initial conditions, and R_0 are the same as in Fig. 3 except $\beta = 0.13576$ and $\delta = 1.804 * 10^{-6}$ to account for a stronger force of infection from the environment (taken from Fig. 6). This larger δ creates stronger dynamical differences between the unforced and forced systems. The speed of oscillation decreases over time. The forced system exhibits noise between cycles. Equilibrium values and steady cycles are reached more quickly for smaller values of γ. Oscillatory behavior is more sustained for γ near 0.5 and larger. Eigenvalues indicate all solutions to the autonomous system will be LAS for $\gamma < 1$. Stability is inconclusive for $\gamma = 1$. Equilibria, maxima, and minima decrease as γ increases. Time between same-strain peaks approaches 1 year as γ increases.

anti-phase damped oscillations as opposed to the coinfection model (Fig. 7).

4. Discussion

The present work highlights the roles played by cross-immunity, transmission pathways, and seasonality in infection dynamics for a multiple serotype model of cholera. Particularly in the case of seasonal forcing, an understanding of the periodicity and phase behavior of undamped oscillatory solutions, which have biological foundation in the Bangladesh data, is key to determining appropriate control measures. To elucidate mechanisms driving cholera serotype dynamics in the host population and in the environment, we extend previously studied models that either consider a single-strain $SIRP$ model or a two-strain SIR model with a cross-immunity component. With $R_0 \leq 1$, the disease will die out regardless of the initial case load or pathogen population in the environment. When $R_0 > 1$, unstable single-strain equilibria and a unique positive coexistence equilibrium appear. Competitive exclusion will not happen, as we prove uniform persistence of both strains in the population. In general, solutions attain the endemic steady state after damped oscillations representing an intrinsic frequency of outbreak waves. Cycling of dominance is observed in some simulations between both serotypes prior to reaching the endemic equilibrium. The inclusion of seasonality, creating a non-autonomous system and forcing periodic

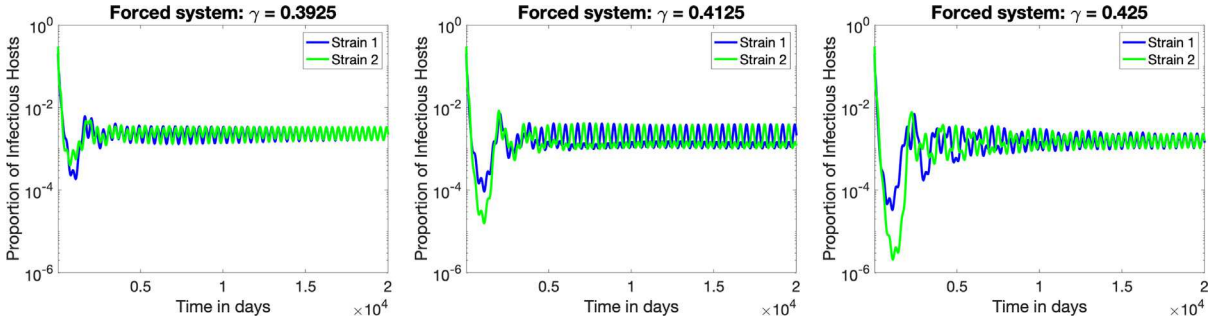

Fig. 5. Exploration of resonance around $\gamma = 0.4$. For $\gamma = 0.3925$ (left) and $\gamma = 0.425$ (right), solutions converge to in-phase oscillations, matching general trend in Fig. 4, with the smaller cross-immunity γ values synchronizing faster, particularly for $\gamma < 0.4$. For $\gamma = 0.4125$ (center), initial dynamics settle into sustained anti-phase oscillations with "pulses" over the long term.

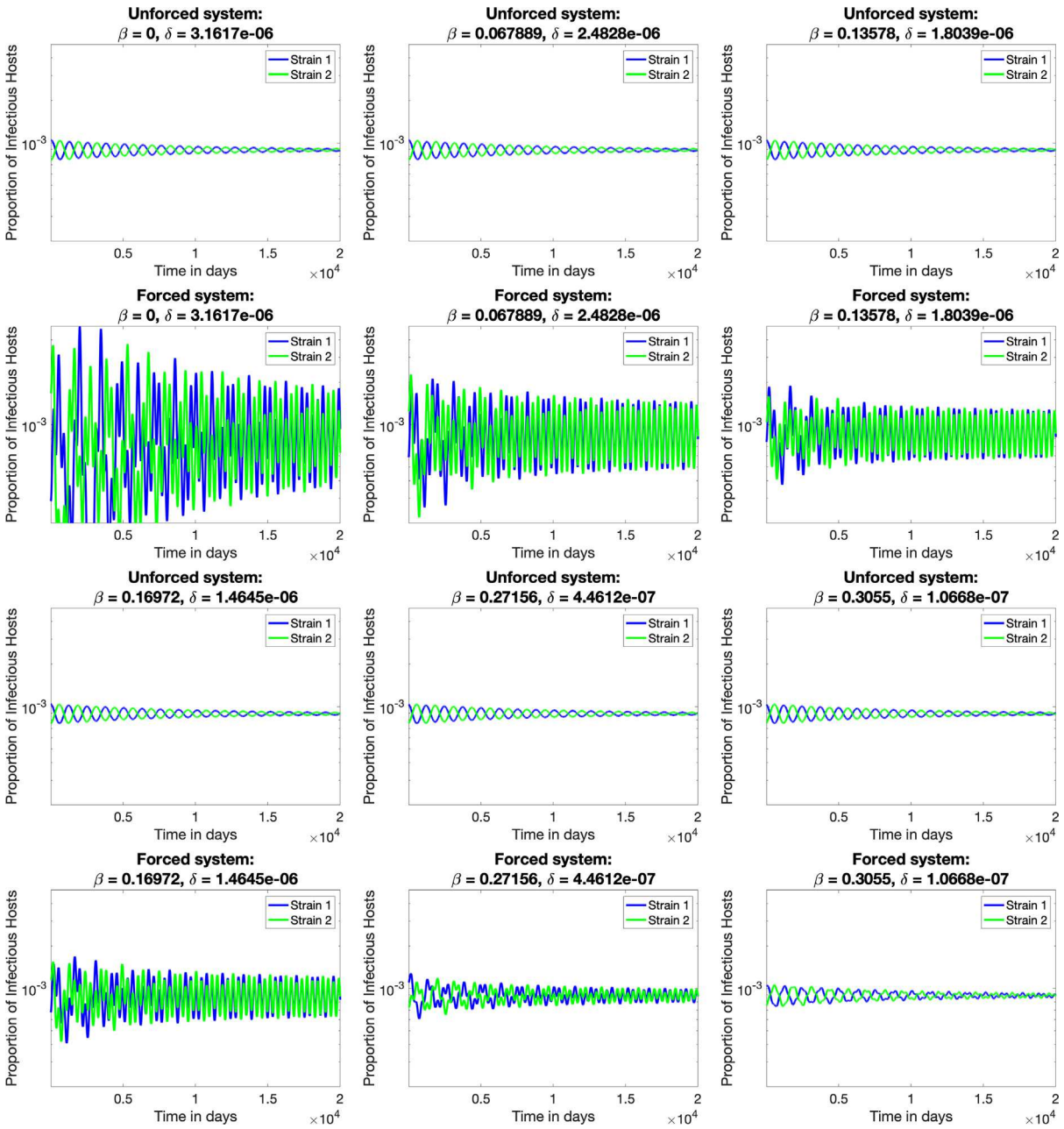

Fig. 6. Compare transmission routes for system (2.3). Parameters are the same as in Fig. 3 with $\gamma = 0.5$, β ranging from 0 to 0.3055 and δ changing in proportion to β, $\delta_0 = 0.1$, keeping R_0 fixed at 3.0016. As β increases and δ decreases, the behavior of the unforced system stays virtually the same. In the forced system, synchronization of solutions slows, and the period of the oscillations increases. Both systems primarily exhibit anti-phase behavior with smaller values of β showing faster synchronization to in-phase behavior.

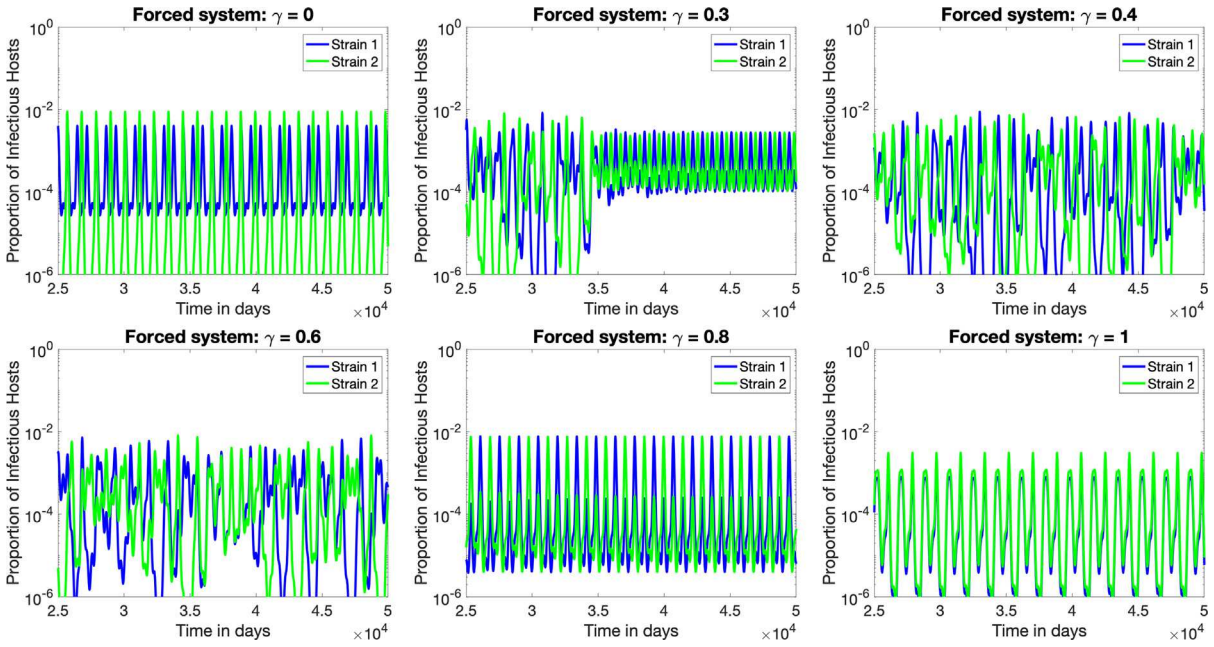

Fig. 7. Coinfection with seasonality. Parameters and initial conditions (with coinfection I added) are the same as in Fig. 3 except for $\delta_0 = 0.15$ and $\alpha = 10^8$. Here, $R_0 = 13.0582$ which is high because we use $\alpha = 10^8$. This was the only α value large enough to sustain the anti-phase dynamics observed. Using $\alpha = 10^6$ as in Fig. 3, all simulations converge to in-phase oscillations (except for $\gamma = 1$).

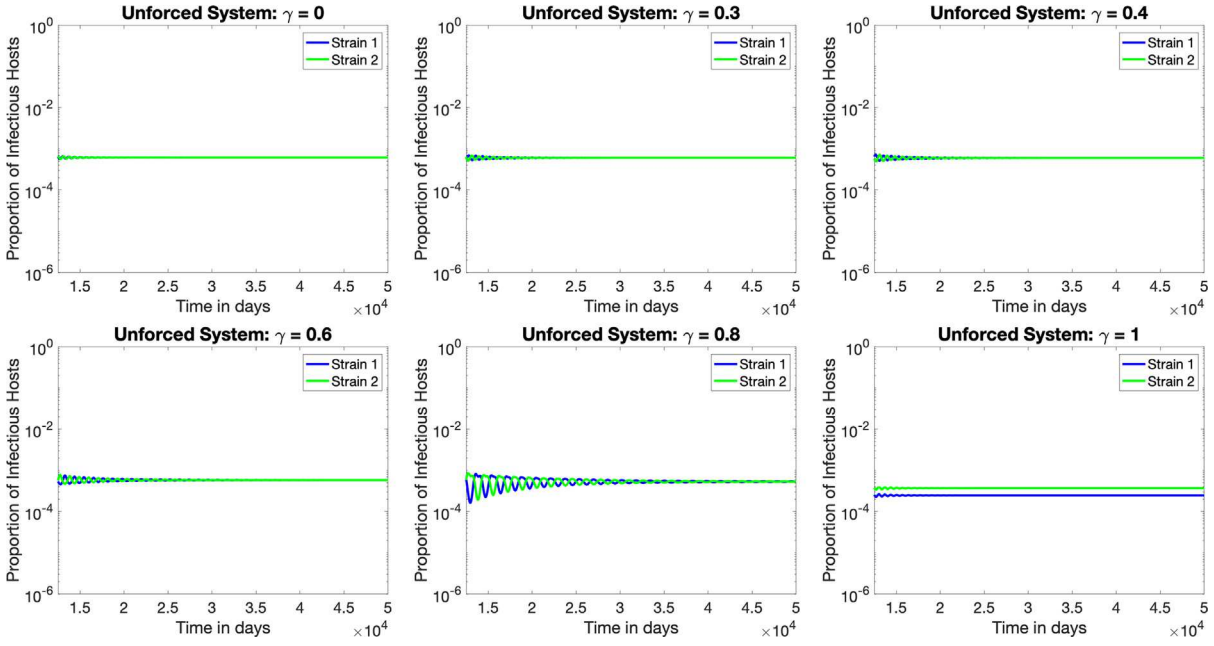

Fig. 8. Coinfection without seasonality. Parameters, initial conditions (with coinfection I added), and R_0 the same as for the non-autonomous system in Fig. 7.

dependence of environment-to-host transmission on the season, allows for more diverse oscillatory dynamics, including in-phase, anti-phase, and out-of-phase cycles and undamped periodic solutions.

The cross-immunity induced from infection by one serotype against the other (parameter γ) impacted both the length of time of damped oscillations and the proportion of infectious hosts. The non-autonomous system (i.e. the autonomous system with the seasonal forcing function) exhibits some anti-phase periodic dynamics which, over time (depending on the degree of seasonal forcing) synchronized the solutions to undamped, in-phase oscillations of a periodic nature. Inclusion of coinfection – included in the motivating two-strain SIR model but excluded in our primary system – leads to more sustained cycling, as shown by simulations with anti-phase, undamped periodic behavior of infectious host solutions similar to the observed behavior in Bangladesh, although we find a resonant case of anti-phase cycling and, more generally, transient anti-phase oscillations for long enough times to match that observed behavior for a range of γ values in our forced model without coinfection. Ultimately, the underlying consideration of a coinfection compartment allows for the presence of a nonlinear term in the infectious host compartments which still allows the seasonal forcing function to contribute periodic dynamics to the behavior of the solutions but which resonates the solutions away from synchronization, magnifying

the intrinsic anti-phase oscillatory mode. Like [8], we observe an association between γ and the two modes (in-phase and anti-phase) of the infectious host solutions. Characterizing the relationship in a more rigorous manner to accurately predict outbreak behavior is a focus of future work.

Varying transmission pathways also affects the structure of the oscillatory behavior within the forced system. Increasing host-to-host transmission β and decreasing environment-to-host transmission δ slowed the synchronizing behavior as well as the time between switches in dominance. Quantifying the relationship between cross-immunity and transmission dynamics can inform best practices for a vaccination control strategy such as when to vaccinate and which strain to vaccinate against. Working to decrease environment-to-host transmission additionally would slow down disease dynamics and reduce the magnitude of an outbreak. Furthermore, the environment can act as a reservoir for a serotype to persist during the lull period after declining from an outbreak or when the other serotype is dominant, after which the seemingly absent serotype can invade the host population by infecting new susceptibles along with recovered individuals with partial cross-immunity [26]. Analysis of the stochastic representation of the system applying a multitype branching process to a continuous time Markov chain has been done around the single-strain equilibria, giving thresholds for the probability of serotype invasion, and environmental parameter δ was found to have a high relative impact on probability of invasion (not shown in this paper). Ultimately, combining environmental and genomic surveillance with better model prediction can allow public health authorities to understand when a serotype may cause an outbreak.

In order to obtain our analytical results, we considered minimal structure for a two strain cholera model with environmental transmission, sequential infection by distinct serotypes, and imperfect cross-immunity. Additional complexities that are realistic to consider include logistic growth of the pathogen, non-symmetric parameters to consider greater strain diversity, terms detailing the mutation from Ogawa to Inaba (and potentially vice-versa), death due to cholera, treatment, and a waning immunity period as well as considering how instances of reinfection affect the immunity of an individual. Stochastic analysis when both strains are persistent around the coexistence equilibrium to determine the probability of a serotype switch in dominance is the subject of future work. Analysis of the system with the seasonal forcing function, particularly determining a persistence result, is still an open problem. Overall, cholera has many complexities that need to be considered to obtain accurate understanding of the dynamics of the disease — transmission through the environment, multiple serotypes with imperfect cross-immunity, and seasonal dependence of transmission are focused on in this model. Furthering our understanding of how these features influence timing, severity, and serotype prevalence of each outbreak is crucial to optimizing control strategies against cholera.

Declaration of competing interest

The authors confirm that there is no financial/personal interest or belief that could affect their objectivity, or if there is, stating the source and nature of that potential conflict.

Acknowledgments

L.L. and C.J.B. acknowledge support by the National Science Foundation grant DMS-1815095.

Appendix A. Proofs of theorems

Proof of Proposition 2.0.1. First, note that the boundary of $\mathbb{R}^{11}_+$ consists of eleven $\mathbb{R}^{10}_+$ hyperplanes, e.g. for the first component S, the boundary is

$$\partial S := \{0\} \times \mathbb{R}_+ \times \mathbb{R}_+ \times \mathbb{R}_+ \times \mathbb{R}_+ \times \mathbb{R}_+ \times \mathbb{R}_+ \times \mathbb{R}_+ \times \mathbb{R}_+ \times \mathbb{R}_+ \times \mathbb{R}_+.$$

Fix a point u on ∂S, so $S = 0$ and all other components of u are positive. Then, the outward unit normal at u is $\vec{n}(u) = (-1, 0, 0, 0, 0, 0, 0, 0, 0, 0, 0)$. Let

$$F(S, I_1, I_2, R_1, R_2, I_{21}, I_{12}, R_{21}, R_{12}, P_1, P_2) = (\dot{S}, \dot{I}_1, \dot{I}_2, \dot{R}_1, \dot{R}_2, \dot{I}_{21}, \dot{I}_{12}, \dot{R}_{21}, \dot{R}_{12}, \dot{P}_1, \dot{P}_2),$$

so $F(u) = (\mu, -(\nu+\mu)I_1, -(\nu+\mu)I_2, \dot{R}_1, \dot{R}_2, \dot{I}_{21}, \dot{I}_{12}, \dot{R}_{21}, \dot{R}_{12}, \dot{P}_1, \dot{P}_2)$.

Hence,

$$\vec{n}(u) \cdot F(u) = -\mu < 0.$$

The same argument, applied to all the boundaries, gives that $\mathbb{R}^{11}_+$ is positively invariant. In fact, we have the existence of a compact, positively invariant subset of $\mathbb{R}^{11}_+$ under our solution flow.

Let $N = S + I_1 + I_2 + R_1 + R_2 + I_{21} + I_{12} + R_{21} + R_{12}$. Then,

$$\dot{N} = \mu(1 - N) \tag{A.1}$$

which gives

$$\begin{aligned} \dot{N} + \mu N &= \mu \\ e^{\mu t}\dot{N} + \mu e^{\mu t} N &= \mu e^{\mu t} \\ \frac{\mathrm{d}e^{\mu t} N}{\mathrm{d}t} &= \mu e^{\mu t} \end{aligned}$$

Integrating both sides gives

$$\begin{aligned} e^{\mu t} N(t) - N_0 &= e^{\mu t} - 1 \\ N(t) &= 1 + (N_0 - 1)e^{-\mu t} \\ N(t) &\le 1. \end{aligned}$$

Hence,

$$\begin{aligned} \dot{P} &:= \dot{P}_1 + \dot{P}_2 \\ &= \alpha_1 I_1 + \alpha_2 I_{21} - r_1 P_1 + \alpha_1 I_2 + \alpha_2 I_{21} - r_2 P_2 \\ &\le \max\{\alpha_i\}(I_1 + I_2 + I_{21} + I_{12}) - \max\{r_i\} P \\ &\le \mathrm{A} - rP. \end{aligned}$$

By the comparison principle, we have that $P(t) \le x(t)$ where $x(t)$ satisfies $\dot{x} = \mathrm{A} - rx$. This has a zero at $M := \frac{\mathrm{A}}{r}$. The phase portrait gives $\limsup_{t\to\infty} x(t) \le M$. Hence,

$$\limsup_{t\to\infty} P(t) \le \limsup_{t\to\infty} x(t) \le M.$$

Therefore, the region

$$\begin{aligned} \Gamma = \{&(S, I_1, I_2, R_1, R_2, I_{21}, I_{12}, R_{21}, R_{12}, P_1, P_2) \\ &\in \mathbb{R}^{11}_+ | S + I_1 + I_2 + R_1 + R_2 + I_{21} + I_{12} + R_{21} + R_{12} \le 1, P_1 + P_2 \le \frac{\mathrm{A}}{r}\} \end{aligned}$$

is positively invariant with respect to system (2.1). Notice also that this shows the system to be well-posed and dissipative. Also, Appendix A gives that $\{(S, I_1, I_2, R_1, R_2, I_{21}, I_{12}, R_{21}, R_{12}, P_1, P_2) \in \mathbb{R}^{11}_+ | N = 1\}$ is invariant.

□

Proof of Theorem 2.1. As in [3,21], we use the method of constructing a Lyapunov function from the next generation method decomposition of our system. We apply the Perron–Frobenius Theorem to a Lyapunov function, then extend the results with LaSalle's Invariance Principle to achieve the desired result.

Let $x = (y_1, y_2, P_1, P_2)^T$ and $x_j = (y_j, P_j)^T$. The system is normalized, so

$$S + (1 - \gamma)R_k \le 1 \tag{A.2}$$

for $k \in [1, 2]$. We can write the second equation of (2.3) as

$$\frac{\mathrm{d}y_j}{\mathrm{d}t} = (\beta y_j + \delta P_j)(S + (1 - \gamma)R_k) - (\nu + \mu)y_j. \tag{A.3}$$

From here, we can rewrite the infectious-pathogen subsystem as

$$\frac{dy_j}{dt} \leq \beta y_j + \delta P_j - (\nu+\mu)y_j \tag{A.4}$$

$$\frac{dP_j}{dt} = \alpha y_j - rP_j. \tag{A.5}$$

Hence,

$$\frac{dx_j}{dt} \leq (F'-V')x_j \tag{A.6}$$

where

$$F' = \begin{pmatrix} \beta & \delta \\ 0 & 0 \end{pmatrix}, \quad V' = \begin{pmatrix} \nu+\mu & 0 \\ -\alpha & r \end{pmatrix}. \tag{A.7}$$

Notice that $\rho(F'(V')^{-1}) = R_0$ where R_0 is the reproduction number described in (2.7). By the Perron–Frobenius Theorem, the irreducible matrix $(V')^{-1}F'$ has a positive left eigenvector $u > 0$ corresponding to eigenvalue $\rho((V')^{-1}F') = \rho(F'(V')^{-1}) = R_0$, i.e. $u^T(V')^{-1}F' = R_0u^T$. We then consider a Lyapunov function

$$L(x) = u^T(V')^{-1}(x_1+x_2). \tag{A.8}$$

Then,

$$\frac{dL}{dt} = \frac{\partial L}{\partial S}\cdot\frac{dS}{dt} + \frac{\partial L}{\partial y_1}\cdot\frac{dy_1}{dt} + \cdots + \frac{\partial L}{\partial P_2}\cdot\frac{dP_2}{dt} \tag{A.9}$$

$$= u^T(V')^{-1}\left(\frac{dx_1}{dt}+\frac{dx_2}{dt}\right) \tag{A.10}$$

$$\leq u^T(V')^{-1}(F'-V')(x_1+x_2) \tag{A.11}$$

$$= (R_0-1)u^T(x_1+x_2). \tag{A.12}$$

Since $R_0 \leq 1$, it follows that $\frac{dL}{dt} \leq 0$. If both $\frac{dL}{dt} = 0$ and $R_0 < 1$, then the last equality on line (A.12) implies $u^T(x_1+x_2) = \mathbf{0}$, i.e. $u_1(y_1+y_2) = 0$ or $u_2(P_1+P_2) = 0$. Since u is an eigenvector, one component is nonzero, so either $y_1 = -y_2$ or $P_1 = -P_2$. Since y_j, $P_j \geq 0$, either $y_1 = y_2 = 0$ or $P_1 = P_2 = 0$. It follows from the second, third, sixth, and seventh equations of the original system that if $y_j = 0$, then $P_j = 0$ and vice versa. Thus, the largest invariant set for which $\frac{dL}{dt} = 0$ is satisfied is $y_1 = y_2 = P_1 = P_2 = 0$. The fourth and fifth equations show global convergence to $R = 0$, and hence to $S = 1$ by the first equation, on the above invariant set. The invariant set is then just $\{(1,0,0,0,0,0,0)\}$. Global asymptotic stability of the DFE in $\mathcal{A}$ follows from LaSalle's Invariance Principle.

When *both* $R_0 = 1$ and $\frac{dL}{dt} = 0$, we have

$$0 = \frac{dL}{dt} \tag{A.13}$$

$$= u^T(V')^{-1}\left(\frac{dx_1}{dt}+\frac{dx_2}{dt}\right) \tag{A.14}$$

$$= u^T(V')^{-1} \times \begin{pmatrix} (\beta y_1+\delta P_1)(S+(1-\gamma)R_2) + (\beta y_2+\delta P_2)(S+(1-\gamma)R_1) - (\nu+\mu)(y_1+y_2) \\ \alpha(y_1+y_2) - r(P_1+P_2), \end{pmatrix} \tag{A.15}$$

and by (A.12) with assumption $R_0 = 1$,

$$0 = (R_0-1)u^T(x_1+x_2) \tag{A.16}$$

$$= u^T(V')^{-1}(F'-V')(x_1+x_2) \tag{A.17}$$

$$= u^T(V')^{-1}\begin{pmatrix} \beta y_1+\delta P_1+\beta y_2+\delta P_2-(\nu+\mu)(y_1+y_2) \\ \alpha(y_1+y_2)-r(P_1+P_2) \end{pmatrix}. \tag{A.18}$$

Thus, we have that (2.21) and (2.24) are both equal to zero. Since $u^T(V')^{-1} > 0$, it follows that

$$(\beta y_1+\delta P_1)(S+(1-\gamma)R_2)+(\beta y_2+\delta P_2)(S+(1-\gamma)R_1) = \beta y_1+\delta P_1+\beta y_2+\delta P_2, \tag{A.19}$$

giving

$$(\beta y_1+\delta P_1)(S+(1-\gamma)R_2-1)+(\beta y_2+\delta P_2)(S+(1-\gamma)R_1-1) = 0.$$

By Appendix A, $(S+(1-\gamma)R_k-1) \leq 0$, and since y_k, P_k are non-negative, we conclude that

$$(\beta y_1+\delta P_1)(S+(1-\gamma)R_2-1) = 0 = (\beta y_2+\delta P_2)(S+(1-\gamma)R_1-1).$$

Without loss of generality, this gives us two cases to consider:

Case 1: $\beta y_1 + \delta P_1 = 0$

In this case, $y_1 = P_1 = 0$ since all populations are nonnegative. It follows that $\frac{dR_1}{dt} \leq -\mu R_1$; on the invariant set, then, $R_1 = 0$. From equation (Appendix A),

$$(\beta y_2+\delta P_2)(S-1) = 0.$$

If $S = 1$, then S is at equilibrium, so $y_2 = P_2 = R_2$. If $\beta y_2 + \delta P_2 = 0$, it follows that $R_2 = 0$ on the invariant set, so $S = 1$. Thus, the invariant set is the singleton $\{(1,0,0,0,0,0,0)\}$.

Case 2: $(S+(1-\gamma)R_2-1) = 0 = (S+(1-\gamma)R_1-1)$

By Proposition 2.0.1, the sum of host populations is one in the positively invariant set $\mathcal{A}$ (2.4). It is easy to see that $S > 0$, so $(S+(1-\gamma)R_2-1) = 0 \Rightarrow S = 1$, and all other components are zero. Thus, the invariant set is the singleton $\{(1,0,0,0,0,0,0)\}$. Then, the DFE is globally asymptotically stable on $\mathcal{A}$, again by LaSalle's Invariance Principle. □

Proof of Lemma 2.2. By (2.9), $R_{inv}^{(k)} > 1$ if and only if $R_0 > 1$ (recall that $\gamma \leq 1$ since it represents cross-immunity). By [20], the single-strain equilibrium E_k is unstable since $R_{inv}^{(k)} > 1$. □

Proof of Theorem 2.3. Without loss of generality, consider the strain 2 boundary where all strain 1 infection components are 0. Our system reduces to

$$\begin{aligned} \frac{dS}{dt} &= -\beta y_2 S - \delta P_2 S + \mu(1-S) \\ \frac{dy_2}{dt} &= \beta y_2 S + \delta P_2 S + (1-\gamma)\beta y_2 R_1 + (1-\gamma)\delta P_2 R_1 - (\nu+\mu)y_2 \\ \frac{dR_1}{dt} &= -(1-\gamma)\beta y_2 R_1 - (1-\gamma)\delta P_2 R_1 - \mu R_1 \\ \frac{dR_2}{dt} &= \nu y_2 - \mu R_2 \\ \frac{dP_2}{dt} &= \alpha y_2 - rP_2 \end{aligned} \tag{A.20}$$

Since $\lim_{t\to\infty} R_1(t) = 0$, the limiting system is equivalent to the system analyzed in [3] with the immunity component and pathogen growth rates taken to be 0. When restricted to this boundary, the system's basic reproduction number is just R_0. The desired result then follows from Theorem 3.4 of [3]. □

Proof of Lemma 2.4. Notice that we can write $\bar{P}_j = \frac{\alpha}{r}y_j$. Solving the equilibrium equations $\dot{y}_1 = 0$ and $\dot{y}_2 = 0$ gives

$$\bar{S} = \frac{1}{R_0} - (1-\gamma)\bar{R}_1, \quad \bar{S} = \frac{1}{R_0} - (1-\gamma)\bar{R}_2. \tag{A.21}$$

It follows that $\bar{R}_1 = \bar{R}_2$.

Then, since $\dot{R}_1 = 0$ and $\dot{R}_2 = 0$, setting $\dot{R}_1 = \dot{R}_2$ and letting $B := \beta + \frac{\alpha\delta}{r}$ gives

$$\nu\bar{y}_1 - (1-\gamma)B\bar{y}_2\bar{R}_1 - \mu\bar{R}_1 = \nu\bar{y}_2 - (1-\gamma)B\bar{y}_1\bar{R}_2 - \mu\bar{R}_2 \tag{A.22}$$

which, since $\bar{R}_1 = \bar{R}_2$, simplifies to

$$(\bar{y}_1-\bar{y}_2)(\nu+(1-\gamma)B\bar{R}_1) = 0. \tag{A.23}$$

Suppose that $\bar{y}_1 \neq \bar{y}_2$. Then, $\bar{R}_1 = -\frac{\nu}{(1-\gamma)B} < 0$. Since the equilibrium is non-negative, we must have $y_1 = y_2$. It follows that $\bar{P}_1 = \bar{P}_2$. □

Solving for the EE:

At this equilibrium, noting that $\bar{P} = \frac{\alpha}{r}\bar{y}$, System (2.2) reduces to

$$\begin{aligned} 0 &= -2\frac{B}{r}\bar{S}\bar{y} + \mu(1-\bar{S}) \\ 0 &= (\bar{S} + \sigma\bar{R})\frac{B}{r} - U \\ 0 &= \nu\bar{y} - \mu\bar{R} - \sigma\frac{B}{r}\bar{R}\bar{y} \end{aligned} \tag{A.24}$$

where $B := \beta r + \alpha\delta$, $\sigma := 1-\gamma$, and $U := \mu + \nu$. From here, we can also write $\bar{S}$ and $\bar{R}$ in terms of $\bar{y}$:

$$\bar{S} = \frac{\mu r}{\mu r + 2B\bar{y}} \text{ and } \bar{R} = \frac{\nu r\bar{y}}{\mu r + \sigma B\bar{y}}. \tag{A.25}$$

We can also write $\bar{y}$ and $\bar{S}$ as

$$\bar{y} = \frac{\mu r(1-\bar{S})}{2B\bar{S}} \text{ and } \bar{S} = \frac{1}{R_0} - \sigma\bar{R}. \tag{A.26}$$

Substituting the expression for $\bar{R}$ into the latter expression for $\bar{S}$ gives

$$\bar{S} = \frac{1}{R_0} - \sigma\frac{\nu r\bar{y}}{\mu r + \sigma B\bar{y}}. \tag{A.27}$$

Finally, substituting this into the latter expression for $\bar{y}$, we obtain a quadratic equation in terms of $\bar{y}$:

$$2\sigma B^2\bar{y}^2 + B(2Ur - \sigma(B-\mu r))\bar{y} + U\mu r^2(1-R_0) = 0. \tag{A.28}$$

The equations in (2.11) follow directly.

Proof of Proposition 2.4.1. First, note that if we have a positive value for $\bar{y}$, then all other corresponding components will be positive as well. Next, we see (A.28) has a positive leading coefficient. Further, its constant term is negative if and only if $R_0 > 1$. Using Descartes Rule of Signs, the quadratic equation has one positive real root and one negative real root. Thus, we have the existence of a unique (positive) coexistence equilibrium.

To determine the exact expressions for the coexistence equilibrium, notice that, since $\gamma < 1$, we have $\sigma < 1$, and

$$Q \geq 2Ur - \sigma(B + \mu r), \tag{A.29}$$

i.e.

$$0 \geq 2Ur - \sigma(B+\mu r) - Q. \tag{A.30}$$

Examining the numerator of $S_{\pm}$, this implies the positive coexistence equilibrium component for $\bar{S}$ is necessarily given by $\bar{S}_+$. The corresponding values for the other equilibrium components then are $\bar{y}_+$, $\bar{R}_+$, and $\bar{P}_+$. Hence, the unique coexistence equilibrium for the reduced 7-equation system is given by $(\bar{S},\bar{y},\bar{y},\bar{R},\bar{R},\bar{P},\bar{P}) = (\bar{S}_+,\bar{y}_+,\bar{y}_+,\bar{R}_+,\bar{R}_+,\bar{P}_+,\bar{P}_+)$. □

A.1. Persistence definitions/theorems and proof of Theorem 2.5

We use the following definitions from [27] (adapted to our system as needed).

Definition Appendix A.1. A map $\phi : [0,\infty)\times\mathbb{R}^7_+ \to \mathbb{R}^7_+$ (so $\phi(t,x_0) := (S(t), y_1(t), y_2(t), R_1(t), R_2(t), P_1(t), P_2(t))$ where $t \in [0,\infty)$, $x_0 \in \mathbb{R}^7_+$, and any component, e.g. $S(t)$, is the solution to the respective compartment of system (2.3) with initial condition x_0) is called a *(global autonomous) semiflow* to system (2.3) if

1. $\phi(0,x) = x$ for all $x \in \mathbb{R}^7_+$.
2. $\phi(t+s,x) = \phi(t,\phi(s,x))$ for all $t,s \in [0,\infty)$ and $x \in \mathbb{R}^7_+$.

Theorem Appendix A.1. *Let $\phi : J\times X \to X$ be a state-continuous semiflow. Assume that ϕ is point-dissipative and asymptotically smooth. Then, there exists a compact attractor of points, namely the closure $\overline{\Omega}(X)$ of $\Omega(X) = \bigcup_{x\in X}\omega(x)$.*

Definition 1. Let $\rho : X \to \mathbb{R}_+$. A semiflow $\phi : J\times X \to X$ is called *uniformly weakly ρ-persistent*, if there exists some $\epsilon > 0$ such that

$$\limsup_{t\to\infty} \rho(\phi_t(x), M) > \epsilon, \ \forall x \in X, \rho(x) > 0.$$

ϕ is called *uniformly (strongly) ρ-persistent*, if there exists some $\epsilon > 0$ such that

$$\liminf_{t\to\infty} \rho(\phi_t(x), M) > \epsilon, \ \forall x \in X, \rho(x) > 0.$$

Theorem Appendix A.2. *[Uniform Weak Persistence Implies Uniform (Strong) Persistence] We set $\sigma(t,x) := \rho(\phi(t,x))$ and make the following assumptions: There exist a subset B of X and a sequence (B_k) of subsets of X such that the following properties hold:*

- *For every $x \in B$, $\sigma(t,x)$ is a continuous function of $t \geq 0$.*
- *There are no $y \in B$, $s,t \in J$ such that $\rho(y) > 0$, $\sigma(s,y) = 0$, and $\sigma(s+t,y) > 0$.*
- *For every $k \in \mathbb{N}$ and every $x \in X$, $\rho(x) > 0$, there exists some $t_k \in J$ such that $\phi(t,x) \in B_k$ for all $t \geq t_k$, $t \in J$.*
- *If (y_k) is a sequence in X with $y_k \in B_k$ for all $k \in \mathbb{N}$, then, after possibly choosing a subsequence, there exists some $y \in B$ such that $\sigma(s,y_k) \to \sigma(s,y)$ as $k \to \infty$, uniformly for s in any set $[0,t]\bigcap J$, $t \in (0,\infty)$.*

Let $J = \mathbb{R}_+$ or $J = \mathbb{Z}_+$. Under the assumptions above, the semiflow ϕ is uniformly ρ-persistent, whenever it is uniformly weakly ρ-persistent.

Definition 2. Let $\emptyset \neq M \subset X$. A neighborhood V of M is called an *isolating neighborhood* of M in X if every compact invariant $K \subset V$ is a subset of M. M is called *isolated* if it has an isolating neighborhood.

Definition 3. Let $C, B \subset X_0$. C is said to be *chained* to B in X_0, written $C \mapsto B$, if there exists a total trajectory ϕ in X_0 with $\phi(0) \notin C\bigcup B$ such that $\phi(-t) \to C$ and $\phi(t) \to B$ as $t \to \infty$. A finite collection $\{M_1,\dots,M_k\}$ of subsets of X_0 is called *cyclic* if, after possibly renumbering, $M_1 \mapsto M_2$ in X_0 or $M_1 \mapsto M_2 \mapsto \dots \mapsto M_j \mapsto M_1$ in X_0 for some $j \in \{2,\dots,k\}$. Otherwise it is called *acyclic*.

Definition 4. A set M in X is called *(weakly ρ-repelling)* if there is no $x \in X$ such that $\rho(x) > 0$ and $\phi(t,x) \to M$ as $t \to \infty$. M is called *uniformly weakly ρ-repelling* if there exists some $\epsilon > 0$ such that

$$\limsup_{t\to\infty} d(\phi_t(x), M) \geq \epsilon \text{ whenever } x \in X, \rho(x) > 0.$$

Theorem Appendix A.3. *[Acyclicity Theorem] Let $\Omega \subset \bigcup_{i=1}^k M_i$ where each $M_i \subset X_0$ is isolated (in X), compact, invariant, and weakly ρ-repelling, $M_i\bigcap M_j = \emptyset$ if $i \neq j$. If $\{M_1,\dots,M_k\}$ is acyclic, then ϕ is uniformly weakly ρ-persistent.*

We are now ready to prove persistence for our system.

Proof of Theorem 2.5.

We follow the methods detailed in [27] by showing the existence of a compact attractor and that the DFE and SSEs are isolated, invariant, acyclic, and repelling. First, note that from Section 2, the system is well-posed and dissipative in $\mathbb{R}^7_+$, giving the existence of a compact attracting set in $\mathbb{R}^7_+$ (Theorem Appendix A.1. We construct the proof using $\rho : \mathbb{R}^7_+ \to \mathbb{R}_+$ with $\rho := \min\{y_1 + P_1, y_2 + P_2\}$, noting that if $\liminf_{t\to\infty}\rho(\phi(t,x)) > \epsilon$, the existence of a compact (indeed, closed) global attractor requires that $\liminf_{t\to\infty} y_1(t)$, $\liminf_{t\to\infty} y_2(t)$, $\liminf_{t\to\infty} P_2(t)$, $\liminf_{t\to\infty} P_2(t) > 0$, i.e. $\liminf_{t\to\infty}\rho(\phi(t,x)) > \epsilon$. We construct the *extinction set* X_0, defined by

$$X_0 = \{x \in \mathbb{R}^7_+ | \rho(\phi(t,x)) = 0 \ \forall t \geq 0\}. \tag{A.31}$$

The invariant set X_0 can be decomposed in terms of "disease-free" and boundary sets (2.10):

$$\begin{aligned} X_0 =& \{x \in \mathbb{R}^7_+ | \rho(\phi(t,x)) = 0 \ \forall t \geq 0\} \\ =& \{(S,0,0,R_1,R_2,0,0) \in \mathbb{R}^7_+\} \cup X_0^{(1)} \cup X_0^{(2)}. \end{aligned} \tag{A.32}$$

In the same manner, $\rho(\phi(t,x))$ must be positive for all $x \in \mathbb{R}^7_+/X_0$. and for all $t > 0$.

Let $\Omega = \bigcup_{x \in X_0} \omega(x)$. We have that $\Omega \subset X_0$ since X_0 is invariant. On each boundary, since the invasion reproduction numbers are greater than 1, the corresponding single-strain equilibrium will be GAS by Theorem 2.3. Then, the only limit points of X_0 are the equilibria E_0 (DFE), E_1 (strain 2 SSE/strain 1 DFE), and E_2 (strain 1 SSE/strain 2 DFE). Thus, $\Omega = \bigcup_{i=0}^2 M_i$, where $M_i = E_i$. Since each M_i is an equilibrium point, each M_i is compact and invariant in $\mathbb{R}^7_+$.

We next examine the linearization of the system in X_0. Since $R_0 > 1$, the DFE is unstable, and both single-strain equilibria are also unstable by Lemma 2.2. Specifically, the Jacobian matrix of each equilibria must have at least one eigenvalue with positive real part. Thus, for any neighborhood V of each equilibria, the linearized system with initial condition $v \in V$ will grow unbounded in the direction of the eigenvector associated with that eigenvalue. By the Hartman-Grobman Theorem, the nonlinear system (2.3) is topologically conjugate to the linearized system in some neighborhood of the given equilibrium. Thus, system (2.3) will also be unbounded, and it follows that each M_i is isolated in $\mathbb{R}^7_+$.

Since $R_0 > 1$, Theorem 2.3 states that on each boundary, the corresponding single-strain equilibrium will be globally asymptotically stable. On the invariant set where $y_1(t) = R_1(t) = P_1(t) = y_2(t) = R_2(t) = P_2(t) = 0$ for all $t \geq 0$, all compartments decouple and go to zero with the exception of $\frac{dS}{dt} = \mu(1-S)$. Thus, S will increase and converge to equilibrium component $\bar{S} = 1$ since the system is normalized. Hence, our DFE is globally asymptotically stable on this set. We will show that asymptotic stability implies that no equilibrium is chained to itself.

Assume an asymptotically stable equilibrium E is chained to itself; that is, suppose there exists a trajectory $\phi(t,x_0)$ such that $x_0 \neq E$ ($\phi(t_0,x_0) = x_0$) and $\phi(t,x_0) \to E$, $\phi(-t,x_0) \to E$ as $t \to \infty$. Since $x_0 \neq E$, fix $\epsilon > 0$ such that $\phi(t,x_0) \notin N_\epsilon(E)$ (the ϵ-neighborhood of E). Since E is asymptotically stable, there exists δ_ϵ such that if $\phi(t_1,x_0) \in N_{\delta_\epsilon}(E)$ for $t_1 \geq 0$, then $\phi(t) \in N_\epsilon(E)$ for all $t \geq t_1$. Since $\phi(-t,x_0) \to E$ as $t \to \infty$, fix $t_2 > t_0$ large enough that $\phi(-t_2,x_0) \in N_{\delta_\epsilon}(E)$. Since E is asymptotically stable, $\phi(t,x_0) \in N_\epsilon(E)$ for all $t \geq -t_2$. This is a contradiction to $x_0 \notin N_\epsilon(E)$ since $t_0 > -t_2$. To show each equilibrium is not chained to itself through another equilibrium, it is sufficient to say that, within each hyperplane on the boundary, the other equilibria do not exist (or a solution would have to go through the origin which cannot happen because it is invariant). Hence, $\bigcup_{i=0}^2 M_i$ is acyclic.

By Theorem Appendix A.3, the last step for the desired result is to show each M_i is weakly ρ-repelling in $\mathbb{R}^7_+$, (see Definition 4 in the appendix). To show this, we follow the methods outlined in [22,28]. Define the stable manifold of equilibrium E_i, $i = 0,1,2$ as

$$W^S(E_i) = \{x_0 \in X | \phi(t,x_0) \underset{t\to\infty}{\to} E_i\} \tag{A.33}$$

Our goal is to show that

$$M := \left(\bigcup_{i=0}^2 W^S(E_i)\right) \cap X_{\text{Int}} = \emptyset. \tag{A.34}$$

By way of contradiction, suppose there exists $x_0 \in M$; that is, suppose there exists

$$x_0 = (S(0), y_1(0), y_2(0), R_1(0), R_2(0), P_1(0), P_2(0)) \tag{A.35}$$

with $y_1(0) \neq 0, y_2(0) \neq 0$, and with $\phi(t,x_0) \underset{t\to\infty}{\to} E_i$ for some fixed i, $i = 0,1,2$. We write $E_i = (\bar{S}, \bar{y}_1, \bar{y}_2, \bar{R}_1, \bar{R}_2, \bar{P}_1, \bar{P}_2)$. Let $\epsilon > 0$. Then, there exists $\delta > 0$ such that if $\|x_0 - E_i\| < \delta$, then $\|\phi(t,x_0) - E_i\| < \epsilon$ for all $t \geq 0$. In other words,

$$\|(S(t)-\bar{S}, y_1(t)-\bar{y}_1, y_2(t)-\bar{y}_2, R_1(t)-\bar{R}_1, R_2(t)-\bar{R}_2, P_1(t)-\bar{P}_1, P_2(t)-\bar{P}_2)\| < \epsilon. \tag{A.36}$$

We recall two points: first, $\bar{S} \leq 1$ for all equilibrium E_i, and second, $\bar{y}_j = \bar{R}_j = \bar{P}_j = 0$ for $j = 1$ or $j = 2$ (or both) by the structure of the three equilibrium. It follows that

$$1 - \epsilon \leq S(t) \leq 1 + \epsilon, \ 0 < y_j(t) < \epsilon, \ 0 < R_j(t) < \epsilon, \ 0 < P_j(t) < \epsilon \tag{A.37}$$

so we can write

$$\frac{dy_j}{dt} \geq \beta(1-\epsilon)y_j - (\nu+\mu)y_j + \delta(1-\epsilon)P_j \tag{A.38}$$

which gives the decoupled matrix system

$$\begin{aligned} \begin{bmatrix} \frac{dy_j}{dt} \\ \frac{dP_j}{dt} \end{bmatrix} &\geq \begin{bmatrix} \beta(1-\epsilon)y_j - (\nu+\mu)y_j + \delta(1-\epsilon)P_j \\ \alpha y_j - rP_j \end{bmatrix} \\ &= \begin{bmatrix} \beta(1-\epsilon) - (\nu+\mu) & \delta(1-\epsilon) \\ \alpha & -r \end{bmatrix} \begin{bmatrix} y_j \\ P_j \end{bmatrix} \end{aligned} \tag{A.39}$$

i.e.

$$\begin{bmatrix} \frac{dy_j}{dt} \\ \frac{dP_j}{dt} \end{bmatrix} \geq [F - V - \epsilon K] \begin{bmatrix} y_j \\ P_j \end{bmatrix} \tag{A.40}$$

where

$$K = \begin{bmatrix} \beta & \delta \\ 0 & 0 \end{bmatrix} \tag{A.41}$$

and F and V are defined as in the next generation method as in [3] (and in [22]). Note that $F - V$ is cooperative and irreducible. Since $R_0 > 1$, $\text{Re}(\lambda) > 0$ where λ is the eigenvalue of $F - V$ with largest real part. For ϵ small enough, $\text{Re}(\lambda_\epsilon) > 1$ where (λ_ϵ is the eigenvalue of $F - V - \epsilon K$ with largest real part). Thus, by the form of the fundamental matrix solution to $\dot{x} = [F - V - \epsilon K]x$, the solution will diverge. By the comparison theorem, y_i and P_i will also diverge. This contradicts $x_0 \in M$, so we have weakly ρ-repelling. Finally, we note the existence of a compact global "persistence attractor" in $\mathbb{R}^7_+/X_0$ by Theorem 5.7 in [27]. Since all infection components in solutions originating in $\mathbb{R}^7_+/X_0$ become positive after $t > 0$, it follows that $\liminf_{t\to\infty} \min\{y_1(t), P_1(t), y_2(t), P_2(t)\} > \epsilon$. □

Appendix B. Analysis of coexistence equilibria when $\gamma = 1$

When $\gamma = 1$, R_1 and R_2 decouple and reduce the system to

$$\begin{aligned} \frac{dS}{dt} &= \mu(1-S) - (\beta y_1 + \delta P_1)S - (\beta y_2 + \delta P_2)S \\ \frac{dy_j}{dt} &= (\beta y_j + \delta P_j)S - (\nu+\mu)y_j \\ \frac{dP_j}{dt} &= \alpha y_j - rP_j. \end{aligned} \tag{B.1}$$

This produces a line of coexistence equilibria defined by

$$\frac{f(S)}{S} = -(\beta + \frac{\delta\alpha}{r})(y_1 + y_2).$$

The corresponding Jacobian, evaluated at the coexistence equilibrium

$$(1/R_0, \bar{y}_1, \bar{y}_2, \frac{\alpha}{r}\bar{y}_1, \frac{\alpha}{r}\bar{y}_2),$$

is

$$J = \begin{pmatrix} -\mu - VY & -\beta/R_0 & -\beta/R_0 & -\delta/R_0 & -\delta/R_0 \\ B\bar{y}_1 & \beta/R_0 - V & 0 & \delta/R_0 & 0 \\ B\bar{y}_2 & 0 & \beta/R_0 - V & 0 & \delta/R_0 \\ 0 & \alpha & 0 & -r & 0 \\ 0 & 0 & \alpha & 0 & -r \end{pmatrix}$$

where $Y := y_1 + y_2$, $B := (\beta + \frac{\alpha\delta}{r})$ and $V := (\nu + \mu)$, so $R_0 = B/V$. The Jacobian is similar to the following matrix:

$$\begin{pmatrix} -\mu - VY & -\beta/R_0 & -\delta/R_0 & -\beta/R_0 & -\delta/R_0 \\ B\bar{y}_1 & \beta/R_0 - V & \delta/R_0 & 0 & 0 \\ 0 & \alpha & -r & 0 & 0 \\ B\bar{y}_2 & 0 & 0 & \beta/R_0 - V & \delta/R_0 \\ 0 & 0 & 0 & \alpha & -r \end{pmatrix},$$

so they will have the same eigenvalues. We use the second matrix to find the eigenvalues.

$$\begin{vmatrix} -\mu - VY - \lambda & -\beta/R_0 & -\delta/R_0 & -\beta/R_0 & -\delta/R_0 \\ B\bar{y}_1 & \beta/R_0 - V - \lambda & \delta/R_0 & 0 & 0 \\ 0 & \alpha & -r - \lambda & 0 & 0 \\ B\bar{y}_2 & 0 & 0 & \beta/R_0 - V - \lambda & \delta/R_0 \\ 0 & 0 & 0 & \alpha & -r - \lambda \end{vmatrix}$$

$$\begin{aligned} =&(-\mu - VY - \lambda)[(\beta/R_0 - V - \lambda)(-r - \lambda) \\ &- \alpha\delta/R_0][(\beta/R_0 - V - \lambda)(-r - \lambda) - \alpha\delta/R_0] \\ &- B\bar{y}_1 \begin{vmatrix} -\beta/R_0 & -\delta/R_0 & -\beta/R_0 & -\delta/R_0 \\ \alpha & -r - \lambda & 0 & 0 \\ 0 & 0 & \beta/R_0 - V - \lambda & \delta/R_0 \\ 0 & 0 & \alpha & -r - \lambda \end{vmatrix} \\ &- B\bar{y}_2 \begin{vmatrix} -\beta/R_0 & -\delta/R_0 & -\beta/R_0 & -\delta/R_0 \\ \beta/R_0 - V - \lambda & \delta/R_0 & 0 & 0 \\ \alpha & -r - \lambda & 0 & 0 \\ 0 & 0 & \alpha & -r - \lambda \end{vmatrix} \\ =&(-\mu - VY - \lambda)[(\beta/R_0 - V - \lambda)(-r - \lambda) - \alpha\delta/R_0]^2 \\ &- B\bar{y}_1[-\beta/R_0(-r - \lambda)[(\beta/R_0 - V - \lambda)(-r - \lambda) - \alpha\delta/R_0] \\ &- \alpha(-\delta/R_0)[(\beta/R_0 - V - \lambda)(-r - \lambda) - \alpha\delta/R_0]] \\ &- B\bar{y}_2[\alpha(-\delta/R_0)[(\beta/R_0 - V - \lambda)(-r - \lambda) - \alpha\delta/R_0] \\ &- (-r - \lambda)(-\beta/R_0)[(\beta/R_0 - V - \lambda)(-r - \lambda) - \alpha\delta/R_0]] \\ =&(-\mu - VY - \lambda)\Delta^2 - B\bar{y}_1[-\beta/R_0(-r - \lambda) - \alpha(-\delta/R_0)]\Delta \\ &- B\bar{y}_2[\alpha(-\delta/R_0) - (-r - \lambda)(-\beta/R_0)]\Delta \end{aligned}$$

where $\Delta := (\beta/R_0 - V - \lambda)(-r - \lambda) - \alpha\delta/R_0$. We show that Δ has an eigenvalue $\lambda = 0$.

$$\begin{aligned} \Delta =&(\beta/R_0 - V - \lambda)(-r - \lambda) - \alpha\delta/R_0 \\ =&\lambda^2 - \lambda(-r + \beta/R_0 - V) - r\beta/R_0 + rV - \alpha\delta/R_0. \end{aligned}$$

The constant term in the polynomial simplifies to

$$-(\alpha\delta + r\beta)/R_0 + rV = -rV + rV = 0,$$

resulting in $\lambda = 0$ as an eigenvalue of J.

Appendix C. Analysis of periodic model

The periodic model with seasonal forcing that we consider in Section 3 is as follows:

$$\begin{aligned} \frac{\mathrm{d}S}{\mathrm{d}t} &= -\beta(y_1 + y_2)S - \delta(t)(P_1 + P_2)S + \mu(1 - S) \\ \frac{\mathrm{d}y_j}{\mathrm{d}t} &= \beta y_j S + \delta P_j S + (1 - \gamma)\beta y_j R_k + (1 - \gamma)\delta(t)P_j R_k - (\nu + \mu)y_j \\ \frac{\mathrm{d}R_j}{\mathrm{d}t} &= \nu y_j - (1 - \gamma)\beta y_k R_j - (1 - \gamma)\delta(t)P_k R_j - \mu R_j \\ \frac{\mathrm{d}P_j}{\mathrm{d}t} &= \alpha y_j - rP_j, \end{aligned} \tag{C.1}$$

where $\delta(t) = \delta(1 + \delta_0 \sin(2\pi t/365.2242))$.

The definition of R_0 for a general class of periodic population dynamic models was first introduced by Bacaer and Guernaoui in 2006 [29]. While a threshold quantity can be often found using Floquet theory, a challenge for defining R_0 in periodic non-autonomous models is that the number of secondary cases caused by an infectious individual depends on the season. The advantage of Bacaer's definition of R_0 is that it can be interpreted as the asymptotic ratio of total infections in two successive generations of the infected population and has the threshold properties of the dominant Floquet multiplier. Wang and Zhao established an equivalent definition of R_0 for the case of compartmental periodic ordinary differential equation models [30], which we will utilize.

Define $F(t) = F$ and V as before in the next generation decomposition (2.5) for R_0 of the autonomous model, where $\delta(t) = \delta$ is now a periodic function. Then the linearized subsystem at the DFE of the periodic system (C.2) can be written as follows:

$$\frac{dx}{dt} = (F(t) - V)x. \tag{C.2}$$

Consider the principal fundamental solution to (C.2), denoted by $\Phi_{F-V}(t)$. The Floquet multipliers of the linear system (C.2) are the eigenvalues of $\Phi_{F-V}(\tau)$. It can be shown that there is a dominant Floquet multiplier, r, which is the spectral radius of $\Phi_{F-V}(\tau)$, i.e.

$$\theta = \rho(\Phi_{F-V}(\tau)). \tag{C.3}$$

Following [30], let $\phi(s)$, which is τ-periodic in s, be an initial periodic distribution of infectious individuals. Given $t \geq s$, $e^{-V(t-s)}F(s)\phi(s)$ gives the distribution of those infected individuals who were newly infected at time s and remain in the infected compartments at time t. Then

$$\psi(t) \equiv \int_{-\infty}^{t} e^{-V(t-s)}F(s)\phi(s)\,ds = \int_0^{\infty} Y(t, t-a)F(t-a)\phi(t-a)\,da$$

is the distribution of cumulative new infections at time t produced by all those infected individuals $\phi(s)$ introduced at times earlier than t.

Let C_τ be the ordered Banach space of all τ-periodic piecewise continuous functions from $\mathbb{R} \to \mathbb{R}^6$, which is equipped with the maximum norm $\|\cdot\|$. Define the linear operator $L : C_\tau \to C_\tau$ by

$$(L\phi)(t) = \int_0^{\infty} e^{-Va}F(t-a)\phi(t-a)\,da, \quad \forall t \in \mathbb{R},\ \phi \in C_\tau.$$

As in [30], we label L the next-infection operator and define the spectral radius of L as the reproduction number:

$$R_0 \equiv \rho(L). \tag{C.4}$$

There is a useful characterization of R_0 as follows. Consider the following linear τ-periodic system

$$\frac{dw}{dt} = \left[-V + \frac{F(t)}{\lambda}\right]w, \quad t \in \mathbb{R} \tag{C.5}$$

with parameter $\lambda \in (0, \infty)$. Denote the principal fundamental solution of (C.5) by $\Phi(t, \lambda)$. Then the following holds

$$\rho(\Phi(\tau, \lambda)) = 1 \Leftrightarrow \lambda = R_0. \tag{C.6}$$

Furthermore, we have the following equivalences:

$$R_0 < 1 \Leftrightarrow \theta < 1 \tag{C.7}$$

$$R_0 > 1 \Leftrightarrow \theta > 1 \tag{C.8}$$

where $\theta = \rho(\Phi_{F-V}(\tau))$.

We will show that R_0 is a threshold quantity that determines whether the disease dies; in particular, the disease-free equilibrium is globally attracting for system (C.2) when $R_0 < 1$.

Theorem Appendix C.1. *Consider the flow $\varphi(t, x)$ of system (C.2). If $R_0 < 1$ and $x \in \mathcal{A}$, then $\varphi(t, x) \to DFE$ as $t \to \infty$.*

Proof. Let $x \in \mathcal{A}$. Consider the solution $\varphi(t, x)$ of periodic system (C.2) with period τ. By the non-negativity of components and bounds of $\mathcal{A}$, in particular by $S + (1-\gamma)R_k \leq 1$ (Appendix A), we obtain the following:

Table D.4
Summary of numerical results: Unforced system.

No coinfection	Previous model agreement
Uniform persistence for $R_0 > 1$	[3]
$\gamma = 1$: line of coexistence equilibria exists	
Oscillations, amplitudes vary w.r.t. γ	[7–9]
Oscillations insensitive to variations in β, δ	
Anti-phase solution behavior with transient oscillations	[7]
Convergence slows as γ increases; threshold at $\gamma \approx 0.4$	
Interannual oscillations occur for $\gamma \approx 0.8$	[7]
Long, transient anti-phase behavior for $0.5 \leq \gamma \leq 0.8$	[8]
Coinfection	
Transient oscillations; convergence to equilibrium for all values of γ	
Out-of-phase behavior for small values of γ; anti-phase behavior appears as γ increases	

Table D.5
Summary of numerical results: Forced system.

No coinfection	Previous model agreement
Oscillation dynamics and caseloads vary wrt γ, β, δ	[7–9]
Increasing (decreasing) β (δ) slows synchronization, increases time between peaks, dampens interannual cycles, and decreases casesloads and amplitude	[8,9]
As γ increased, system resembles unforced system in oscillatory speed	
Anti-phase oscillations synchronize to in-phase oscillations depending on magnitude of δ_0	
0.4: threshold for γ where synchronization to in-phase oscillations slows	
$0.3975 \leq \gamma \leq 0.4125$ exhibits resonance with anti-phase oscillations	[9]
In-phase oscillations more common than anti-phase	[9]
Synchronization slows as γ increases	
Interannual oscillations for $0.5 < \gamma < 1$	[8,9]
Long, transient anti-phase behavior for $0.5 \leq \gamma \leq 0.8$	[7–9]
Coinfection	
Sustained, anti-phase oscillatory dynamics for $\gamma \in (0, 0.2) \cup (0.6, 0.8)$; the second range aligns similarly with the range for sustained anti-phase behavior in the system without coinfection	[7–9]

$$\begin{aligned} \frac{\mathrm{d}y_j}{\mathrm{d}t} &\leq \beta y_j + \delta(t) P_j - (\nu + \mu) y_j \\ \frac{\mathrm{d}P_j}{\mathrm{d}t} &= \alpha y_j - r P_j. \end{aligned} \tag{C.9}$$

Consider the principal fundamental solution of the right-hand side of system (C.9) as a function of ϵ: $\Phi(t, \epsilon)$. Then $\rho(\Phi(\tau, 0)) = \theta$. Since $\Phi(\tau, \epsilon)$ is continuous with respect to ϵ, for ϵ sufficiently small, $\theta(\epsilon) = \rho(\Phi(\tau, \epsilon)) < 1$ since $\theta(0) = \theta < 1$ by (C.7). The matrix $B(t, \epsilon)$, where $B(t, \epsilon)$ represents the right-hand side of (C.9) as a linear vector field, is quasi-positive. Without loss of generality, we can assume the non-diagonal entries of $B(t, \epsilon)$ are positive. If any are zero, add a sufficiently small constant to that entry, and the spectral radius of interest will still fall below unity, and inequality (C.9) will still hold. Thus the matrix $\Phi(\tau, \epsilon)$ will be strictly positive (since the vector field will point away from the boundary). Then, by the Perron–Frobenius Theorem, we find that $\theta(\epsilon)$ is a simple eigenvalue with strictly positive eigenvector v. Hence $z(t) \equiv \Phi(t, \epsilon)v = q(t)e^{\xi t}$ where $\xi = \frac{1}{\tau}\ln(\theta(\epsilon))$ and $q(t)$ is τ-periodic. So $z(t) \to 0$ as $t \to \infty$. Since $B(t, \epsilon)$ is quasi-positive, subsystem (C.9) forms a comparison system using Theorem 1.2 in [31]. Choose a constant c such that $cv \geq x_0$, where $x_0 = \varphi(0, x_0)$. Then $cz(t) \geq \varphi(t, x_0)$ for all $t \geq 0$. Hence $y_i(t) \to 0$ and $P_i(t) \to 0$ as $t \to \infty$ for $i = 1, 2$ since $cz(t) \to 0$. Then, for any $\epsilon > 0$ and sufficiently large time t,

$$\mu(1 - S) - \epsilon \leq \frac{\mathrm{d}S}{\mathrm{d}t}, \quad \frac{\mathrm{d}R_j}{\mathrm{d}t} \leq \epsilon - \mu R_j.$$

Then, because $S + (1 - \gamma)R_j \leq 1$, another application of the comparison system principle yields $\overline{S}^{\epsilon} \leq S_i(t) \leq \overline{S}$ and $\overline{R}_j^{\epsilon} \geq R_j(t) \geq 0$ for t sufficiently large, where $\overline{S}^{\epsilon} \to 1$ and $\overline{R}_j^{\epsilon} \to 0$ as $\epsilon \to 0$. The result follows upon taking limit as $\epsilon \to 0$. □

We note that whether uniform persistence of the disease can be established when $R_0 > 1$ is an open question for the periodic serotype model (C.2). Because the boundary set contains single-strain periodic systems whose global behavior is not easily determined when $R_0 > 1$, uniform persistence is a highly non-trivial problem.

Appendix D. Summary and comparison of numerical results

See Tables Tables D.4 and D.5

References

[1] E.K. Lipp, A. Huq, R.R. Colwell, Effects of global climate on infectious disease: the Cholera model, Clin. Microbiol. Rev. 15 (4) (2002) 757–770.
[2] C.T. Codeço, Endemic and epidemic dynamics of Cholera: the role of the aquatic reservoir, BMC Infect. Dis. 1 (1) (2001) 1–14.
[3] M. Bani-Yaghoub, R. Gautam, Z. Shuai, P. Van Den Driessche, R. Ivanek, Reproduction numbers for infections with free-living pathogens growing in the environment, J. Biol. Dyn. 6 (2) (2012) 923–940.
[4] A.R. Tuite, J. Tien, M. Eisenberg, D.J. Earn, J. Ma, D.N. Fisman, Cholera epidemic in Haiti, 2010: using a transmission model to explain spatial spread of disease and identify optimal control interventions, Ann. Intern. Med. 154 (9) (2011) 593–601.
[5] E.C. Lee, M.R. Kelly Jr., B.M. Ochocki, S.M. Akinwumi, K.E. Hamre, J.H. Tien, M.C. Eisenberg, Model distinguishability and inference robustness in mechanisms of cholera transmission and loss of immunity, J. Theoret. Biol. 420 (2017) 68–81.
[6] Z. Shuai, P. Van den Driessche, Global dynamics of Cholera models with differential infectivity, Math. Biosci. 234 (2) (2011) 118–126.
[7] K. Koelle, M. Pascual, M. Yunus, Serotype cycles in Cholera dynamics, Proc. R. Soc. B Biol. Sci. 273 (1603) (2006) 2879–2886.
[8] M. Kamo, A. Sasaki, The effect of cross-immunity and seasonal forcing in a multi-strain epidemic model, Physica D 165 (3–4) (2002) 228–241.
[9] B. Adams, M. Boots, The influence of immune cross-reaction on phase structure in resonant solutions of a multi-strain seasonal SIR model, J. Theoret. Biol. 248 (1) (2007) 202–211.

[10] S.L. Karlsson, N. Thomson, A. Mutreja, T. Connor, D. Sur, M. Ali, J. Clemens, G. Dougan, J. Holmgren, M. Lebens, Retrospective analysis of serotype switching of Vibrio cholerae O1 in a cholera endemic region shows it is a non-random process, PLoS Negl. Trop. Dis. 10 (10) (2016) e0005044.
[11] T.K. Paisie, M.N. Cash, M.S. Tagliamonte, A. Ali, J.G. Morris Jr., M. Salemi, C. Mavian, Molecular basis of the toxigenic Vibrio cholerae O1 serotype switch from Ogawa to Inaba in Haiti, Microbiol. Spectr. 11 (1) (2023) e03624–22.
[12] A.A. Koepke, I.M. Longini Jr., M.E. Halloran, J. Wakefield, V.N. Minin, Predictive modeling of Cholera outbreaks in Bangladesh, Ann. Appl. Stat. 10 (2) (2016) 575.
[13] L. Wang, Y. Zhou, J. He, B. Zhu, F. Wang, L. Tang, M. Kleinsasser, D. Barker, M.C. Eisenberg, P.X. Song, An epidemiological forecast model and software assessing interventions on the COVID-19 epidemic in China, J. Data Sci. 18 (3) (2020) 409–432.
[14] U.H. Stroeher, L.E. Karageorgos, R. Morona, P.A. Manning, Serotype conversion in Vibrio cholerae O1, Proc. Natl. Acad. Sci. 89 (7) (1992) 2566–2570.
[15] J.H. Tien, H.N. Poinar, D.N. Fisman, D.J. Earn, Herald waves of Cholera in nineteenth century London, J. R. Soc. Interface 8 (58) (2011) 756–760.
[16] I. Levade, Y. Terrat, J.-B. Leducq, A.A. Weil, L.M. Mayo-Smith, F. Chowdhury, A.I. Khan, J. Boncy, J. Buteau, L.C. Ivers, et al., Vibrio cholerae genomic diversity within and between patients, Microbial Genom. 3 (12) (2017).
[17] K.M. Pepin, K. Lambeth, K.A. Hanley, Asymmetric competitive suppression between strains of Dengue virus, BMC Microbiol. 8 (2008) 1–10.
[18] A. Wu, V.T. Mihaylova, M.L. Landry, E.F. Foxman, Interference between Rhinovirus and Influenza A virus: a clinical data analysis and experimental infection study, Lancet Microbe 1 (6) (2020) e254–e262.
[19] W.E. Woodward, Cholera reinfection in man, J. Infect. Dis. 123 (1) (1971) 61–66.
[20] O. Diekmann, J. Heesterbeek, M.G. Roberts, The construction of next-generation matrices for compartmental epidemic models, J. R. Soc. Interface 7 (47) (2010) 873–885.
[21] Z. Shuai, P. van den Driessche, Global stability of infectious disease models using Lyapunov functions, SIAM J. Appl. Math. 73 (4) (2013) 1513–1532.
[22] D. Posny, J. Wang, Modelling Cholera in periodic environments, J. Biol. Dyn. 8 (1) (2014) 1–19.
[23] M.C. Eisenberg, G. Kujbida, A.R. Tuite, D.N. Fisman, J.H. Tien, Examining rainfall and Cholera dynamics in Haiti using statistical and dynamic modeling approaches, Epidemics 5 (4) (2013) 197–207.
[24] M.C. Eisenberg, S.L. Robertson, J.H. Tien, Identifiability and estimation of multiple transmission pathways in Cholera and Waterborne disease, J. Theoret. Biol. 324 (2013) 84–102.
[25] D.M. Hartley, J.G. Morris Jr., D.L. Smith, Hyperinfectivity: a critical element in the ability of V. Cholerae to cause epidemics? PLoS med. 3 (1) (2006) e7.
[26] C.N. Mavian, M.S. Tagliamonte, M.T. Alam, S.N. Sakib, M.N. Cash, M. Moir, J.P. Jimenez, A. Riva, E.J. Nelson, E.T. Cato, et al., Ancestral origin and dissemination dynamics of reemerging toxigenic vibrio cholerae, haiti, Emerging Infectious Diseases 29 (10) (2023) 2072–2082.
[27] H.L. Smith, H.R. Thieme, Dynamical Systems and Population Persistence, Vol. 118, American Mathematical Soc., 2011.
[28] C.J. Browne, R.J. Smith, L. Bourouiba, From regional pulse vaccination to global disease eradication: insights from a mathematical model of poliomyelitis, J. Math. Biol. 71 (1) (2015) 215–253.
[29] N. Bacaër, S. Guernaoui, The epidemic threshold of vector-borne diseases with seasonality: the case of cutaneous leishmaniasis in Chichaoua, Morocco, J. Math. Biol. 53 (3) (2006) 421–436.
[30] W. Wang, X.-Q. Zhao, Threshold dynamics for compartmental epidemic models in periodic environments, J. Dynam. Differential Equations 20 (2008) 699–717.
[31] M. Kirkilionis, S. Walcher, On comparison systems for ordinary differential equations, J. Math. Anal. Appl. 299 (1) (2004) 157–173.